The oceanic sink for anthropogenic CO_2 from 1994 to 2007

Nicolas Gruber (1), Dominic Clement (1), Brendan R. Carter (2,17), Richard A. Feely (2), Steven van Heuven (3), Mario Hoppema (4), Masao Ishii (5), Robert M. Key (6), Alex Kozyr (7), Siv K. Lauvset (8,12), Claire Lo Monaco (9), Jeremy T. Mathis (10), Akihiko Murata (11), Are Olsen (12), Fiz F. Perez (13), Christopher L. Sabine (14), Toste Tanhua (15), and Rik Wanninkhof (16)

1. Environmental Physics, Institute of Biogeochemistry and Pollutant Dynamics, ETH Zurich, Zurich, Switzerland.

2 National Oceanic and Atmospheric Administration, Pacific Marine Environmental Laboratory, Seattle, USA.

3 Centre for Isotope Research, Faculty of Science and Engineering, University of Groningen, the Netherlands.

4 Alfred Wegener Institute, Helmholtz Centre for Polar and Marine Research, Bremerhaven, Germany.

5 Meteorological Research Institute, Japan Meteorological Agency , Tsukuba, Japan.

6 Atmospheric and Oceanic Sciences, Princeton University, Princeton, NJ, USA.

7 NOAA National Centers for Environmental Information, Silver Spring, USA.

8 NORCE Norwegian Research Centre, Bjerknes Centre for Climate Research, Bergen, Norway.

9 LOCEAN, CNRS, Sorbonne Université, Paris, France.

10 National Oceanic and Atmospheric Administration, Arctic Research Program, Silver Spring, USA.

11 Research and Development Center for Global Change, Japan Agency for Marine-Earth Science and Technology,

12 Geophysical Institute, University of Bergen and Bjerknes Centre for Climate Research, Norway.

13 Instituto de Investigaciones Marinas, CSIC (IIM-CSIC), Vigo, Spain

14 Department of Oceanography, University of Hawai`i at Manoa, Honolulu, USA.

15 GEOMAR Helmholtz Centre for Ocean Research Kiel, Kiel, Germany

16 National Oceanic and Atmospheric Administration, Atlantic Oceanographic and Meteorological Laboratory, Miami, USA.

17 Joint Institute for the Study of the Atmosphere and Ocean, University of Washington, Seattle, USA

We quantify the oceanic sink for anthropogenic CO_2 over the period 1994 to 2007 using observations from the global repeat hydrography program and contrasting them to observations from the 1990s. Using a linear regression-based method, we find a global increase in the anthropogenic CO_2 inventory of 34±4 Pg C between 1994 to 2007. This is equivalent to an average uptake rate of 2.6±0.3 Pg C yr^{-1} and represents 31±4 % of the global anthropogenic CO_2 emissions over this period. While this global ocean sink estimate is consistent with the expectation of the ocean uptake having increased in proportion to the rise in atmospheric CO_2, substantial regional differences in storage rate are found, likely owing to climate variability driven changes in ocean circulation.

Using observations from the first global survey of inorganic carbon in the ocean conducted as part of the World Ocean Circulation Experiment (WOCE)/Joint Global Ocean Flux Study (JGOFS) programs during the 1980s and early 1990s, Sabine et al.(*1*) estimated that the ocean has taken up 118±18 Pg (1Pg = 10^{15}g) of anthropogenic carbon, C_{ant}, from the atmosphere from the beginning of the industrial revolution to the mid 1990s. Anthropogenic carbon represents the additional inorganic carbon present in the ocean-atmosphere system as a consequence of human emissions to the atmosphere (*2*, *3*) through the burning of fossil fuel, the production of cement, and land use change (*4*, *5*). We distinguish this anthropogenic component from the fluxes and storage changes associated with natural CO_2, i.e., the quantity of carbon in the atmosphere-ocean system that existed already in preindustrial times (*6*). Here, using novel methods and new high quality ocean observations collected since 2003 on repeat hydrographic cruises (*7*), we extend the analysis of Sabine et al (*1*) to 2007. In particular, we reconstruct the increase in the oceanic storage of C_{ant} between 1994 and 2007 and contrast this to the expected change given the continued increase in atmospheric CO_2.

Detecting the change in anthropogenic CO_2

We use the data synthesized by the Global Ocean Data Analysis Project version 2 (GLODAPv2)(*8*) and the recently developed eMLR(C*) method(*9*) to identify the change in C_{ant} ($\Delta_t C_{ant}$) between the WOCE/JGOFS (nominal 1994) and the Repeat Hydrography/GO-SHIP (nominal 2007) periods *(see supplement for details, Fig S3-5)*. This novel method builds on the extended Multiple Linear Regression (eMLR) approach(*10*), which was designed to separate $\Delta_t C_{ant}$ from any natural CO_2 driven change in dissolved inorganic carbon (*DIC*). The eMLR(C*) method has been extensively tested with synthetic data from a biogeochemical model (*9*), demonstrating its ability to reconstruct $\Delta_t C_{ant}$ with high accuracy at global and basin scales. These tests also revealed that sub-basin scales are less well resolved, especially

in regions characterized by high temporal variability. To quantify the uncertainties in the reconstructions, we used the spread from a Monte Carlo technique and an ensemble of 14 sensitivity studies (*see supplement for details*).

Global distribution

The global, vertical distribution of $\Delta_t C_{ant}$ between 1994 and 2007 reveals the strong gradients that are characteristic for a passive conservative tracer invading the ocean from the surface (Figure 1). In the upper 100 m, C_{ant} increased, on average, by 14 $\mu mol\ kg^{-1}$ over this period, close to the expected level given the rise in atmospheric CO_2 and the ocean's buffer capacity(*11*). Below that, $\Delta_t C_{ant}$ decreases rapidly with depth, reaching half of the surface value at 375 m, and one tenth of it at 1000 m. Half of the global $\Delta_t C_{ant}$ signal is found in the top 400 m, more than 75% above 1000 m, and only about 7% between 2000 and 3000 m.

There are strong spatial variations in the vertical penetration of $\Delta_t C_{ant}$ (Figure 1), reflecting the differences in the efficacy with which the surface signal is transported and mixed down by the large-scale overturning circulation (*1*, *3*, *12–14*). As transport occurs primarily along sloping neutral density surfaces, (*15*), it is instructive to investigate the distribution of $\Delta_t C_{ant}$ on such iso-surfaces (Figure 2). The relatively shallow surfaces associated with mode waters (such as the neutral surface 26.60 kg m^{-3})(*16*) are ventilated on timescales of a few decades or less, such that the anthropogenic CO_2 signal is transported rather effectively from the outcrops at the mid to high latitudes toward the ocean's interior (Figure 2a). In contrast, substantial changes in C_{ant} on the deeper (~1000 m in the mid and low latitudes) 27.40 kg m^{-3} neutral surface are essentially limited to the regions close to the outcrop (Figure 2b). This reflects the decade to century-long ventilation ages of the water masses occupying this neutral surface, consisting, in the Southern Hemisphere, primarily of Antarctic Intermediate Water. Despite its limited horizontal reach, the downward transport of the $\Delta_t C_{ant}$ signal along this neutral surface from the Southern Ocean outcrop leads to the 2nd deepest penetration of $\Delta_t C_{ant}$ anywhere in the ocean (Figure

1). The deepest penetration is found in the North Atlantic, where the downward spreading of newly formed North Atlantic Deep Water (NADW) causes a $\Delta_t C_{ant}$ with a maximum of 5 μmol kg^{-1} below 1000 m. The rapid southward spreading of NADW between about 1500 and 2500 m transports this elevated $\Delta_t C_{ant}$ into the South Atlantic. The corresponding process is much less vigorous and deep reaching in the North Pacific, as there is no deep water formation there. This leads to a shallow penetration by mode and intermediate waters.

These regional differences in the vertical penetration cause large spatial variations in the column inventory of $\Delta_t C_{ant}$, i.e., the change in C_{ant} integrated vertically from the surface down to 3000 m (Figure 3a). Large parts of the mid-latitude North Atlantic increased their anthropogenic CO_2 loads by 16 ±1 mol C m^{-2} or more between 1994 and 2007. This corresponds to an average storage rate of 1.2 ±0.1 mol C m^{-2} yr^{-1}; twice the global mean storage rate of 0.65 ±0.08 mol m^{-2} yr^{-1}. Large changes are also found along a broad zonal band in the mid-latitudes of the Southern Hemisphere, with maximum values above 15 ±2 mol m^{-2} throughout much of the South Atlantic, and progressively smaller values going eastward into the Indian and Pacific Oceans. This reflects the deep, but spatially variable penetration of C_{ant} into the thermoclines of these basins induced by downward transport by mode and intermediate waters (*17*, *18*) (cf. Figure 1), i.e., the upper cell of the meridional overturning circulation in the southern hemisphere (*19*).

In contrast to the regions with high accumulation, the low column inventory changes in the region south of 60°S stand out. The average change in storage there is less than 4 ±2 mol m^{-2}, corresponding to a rate of only 0.30±0.15 mol m^{-2} yr^{-1}, i.e., less than half of the global mean. This low storage rate is associated with the lower cell of the meridional overturning circulation(*19*). First, the upwelling of old waters with low concentrations of C_{ant} (cf. Figure 1) around the Antarctic Polar Front prevents a substantial accumulation of C_{ant} there. Second, there is little downward transport associated with the downward component of the lower cell, likely owing to the physical blocking of the air-sea exchange of CO_2 by sea-ice in the Antarctic zone and

the relatively short residence time of these waters at the surface(*20*). This contrasts strongly with the upper overturning cell, which takes up a lot of anthropogenic CO_2 from the atmosphere, but quickly transports it northward into the band of high storage between 50°S and 30°S (*14*, *17*, *21*).

Global and Regional Inventory Change

Integrated globally and down to a depth of 3000 m, we estimate a change in the inventory of oceanic anthropogenic CO_2 of 31.2±4 Pg C for the period 1994 to 2007 (Tables 1 and S3). To this we add the uptake and storage by regions outside our gridded domain, namely the Mediterranean Sea and the Arctic Ocean, which are estimated to account for ~1.5 Pg C (*22–24*). We add an additional ~1 Pg C to our estimate to account for the accumulation of C_{ant} below 3000 m, estimated from the fraction of C_{ant} found below that depth in 1994 in the observational estimates (*1*) (see also (*25*)) and from the fraction modelled for the 1994 to 2007 period (*14*). This yields a global oceanic storage increase of anthropogenic CO_2 of 34±4 Pg C, which equals a mean annual uptake rate of 2.6 ±0.3 Pg C yr^{-1} over the 1994 to 2007 period.

The individual ocean basins and hemispheres contribute very differently to both the global inventory and its uncertainty (Table 1). Between the hemispheres, the majority (60±11 %) of the increase in C_{ant} is found in the southern hemisphere (Table 1). Between the basins, the storage in the Pacific (39±4%) and Atlantic (35±4%) has increased by roughly equal amounts, while the contribution of the Indian Ocean is much smaller (21±10%). While this smaller storage in the Indian ocean reflects its fractional area coverage, the areal storage in the Atlantic is nearly twice that in the Pacific, primarily reflecting the differences in the uptake and downward transport in the high northern latitudes of these two basins. The largest uncertainty stems from the Indian Ocean primarily as a result of the poor data coverage since 2000 (Figure S1b).

Adding the 34±4 Pg C increase between 1994 and 2007 to the 118±19 Pg C estimated for the change between the preindustrial period and 1994(*1*) yields a global ocean storage for 2007 of 152±20 Pg C. Extrapolating this estimate linearly to the year 2010

147 gives an inventory of 160±20 Pg C, which is consistent with the "best" estimate
148 provided by Khatiwala et al. (*13*) of 155±31 Pg C, obtained by combining models and
149 other constraints. Our estimate confirms also the results of a recent diagnostic model
150 (*14*), which simulated a cumulative storage of about 155 to 161 Pg C for 2010. Our
151 estimate stands out by its use of inorganic carbon measurements as the foundation to
152 determine anthropogenic CO_2 inventories, whereas the other referenced studies
153 employed indirect or model-based methods. Our approach also implicitly includes the
154 effect of a time changing ocean circulation, while the indirect estimates of refs (*14*,
155 *26*) assume a steady-state ocean circulation.
156
157 The eMLR(C*)-based estimates of $\Delta_t C_{ant}$ compare overall well with other regional
158 data-based analyses of the change in anthropogenic CO_2 conducted so far, both in
159 terms of the vertical distributions and the column inventories (*see supplementary*
160 *material*). Our data-based storage rates for the period 1994 to 2007 are also in good
161 agreement with those recently inferred from a diagnostic model of the ocean
162 circulation (*21*) (Figure S6).

163 ***Comparison with the JGOFS/WOCE era reconstructions***

164 The column inventory change between 1994 and 2007 (Figure 3a) is spatially well
165 correlated (r^2 =0.68) with the total inventory of anthropogenic CO_2 in 1994 (Figure
166 3b) (*1*). This is as expected from the nearly exponential and multi-decadal nature of
167 the anthropogenic perturbation of the global carbon cycle. This results in a "transient
168 steady-state"(*27*), which implies - for an ocean with invariant circulation and mixing -
169 that the change of anthropogenic CO_2 over any time period t_1 to t_2 is linearly related to
170 the amount of anthropogenic CO_2 at the initial time, t_1, i.e., $\Delta_t C_{ant}(t_2\text{-}t_1) \approx \alpha \cdot C_{ant}(t_1)$
171 (*28*). We estimate the proportionality α from theoretical considerations for the period
172 1994 through 2007 and obtain a value of α =0.28±0.02 (*see supplementary material*).
173 This value varies little by region, but it varies substantially in time. This theoretically
174 estimated value is statistically indistinguishable from the ratio of the global change in

inventory between 1994 and 2007 (34±4 Pg C) and the inventory in 1994 (118±19 Pg C). This implies that, to first order, the global ocean has continued to take up anthropogenic CO_2 from the atmosphere at a rate expected from the increase in atmospheric CO_2, i.e., there is no indication of a major change in the uptake over the 1994-2007 period relative to the long-term mean.

On a regional basis, however, the reconstructed distribution of Δ_tC_{ant} differs from that inferred from the C_{ant} distribution in 1994 and the assumption of a transient steady-state (Figure 3c). We interpret these differences, i.e., the anomalous accumulation of C_{ant} ($\Delta_tC_{ant}^{anom} = \Delta_tC_{ant} - \alpha \cdot C_{ant)}$ to be primarily the result of variations in ocean circulation. But care must be taken when interpreting $\Delta_tC_{ant}^{anom}$, since the associated uncertainties accumulate the errors from all terms, i.e., Δ_tC_{ant}, α, and C_{ant}. As shown in the supplementary material, the most important source of error is the reconstruction of Δ_tC_{ant} itself. In particular, tests with synthetic data from an ocean biogeochemical model showed that while the eMLR(C*) method generally works well, changes in ocean circulation tend to lead to biases in the reconstructed $\Delta_tC_{ant,}$ which directly impact the inferred $\Delta_tC_{ant}^{anom}$ (*9*). However, these tests also revealed that the method is still able to recover the most important signals associated with $\Delta_tC_{ant}^{anom}$, especially in the North Atlantic. The error is largest in the North Pacific, yet across the globe, more than 50% of the modelled variance in $\Delta_tC_{ant}^{anom}$ at basin-scales is correctly recovered. Globally, the bias of the recovered $\Delta_tC_{ant}^{anom}$ is essentially zero.

The most prominent anomaly is found in the North Atlantic, where the reconstructed change in inventory over the entire basin is 20% smaller than that predicted by the transient steady state (Figure 3c). This anomaly, likely robust given that it was well recovered in the tests with synthetic data, characterizes nearly the entire water column (Figure 4a). The strongest $\Delta_tC_{ant}^{anom}$ are found in the subpolar gyre and within the Subpolar Mode Water and in the Intermediate Water, both belonging to the water masses with the highest burden of anthropogenic CO_2(*10*, *29*). This lower-than-expected increase in storage in the North Atlantic during the 1990s and early 2000 has been described previously (*29–31*) and was attributed to the slow-down and reorganization of the North Atlantic overturning circulation at that time, which led to

a reduction in the downward transport of C_{ant}(*29*, *31*). This slowdown was probably temporary, as indicated by the more recent rapid increase in C_{ant} in the Irminger Sea(*32*).

The anomalously low accumulation in the North Atlantic between 1994 and 2007 co-occurred with an anomalously high accumulation in the South Atlantic, such that the storage change of the entire Atlantic remained very close to the expected one. Even though we are somewhat less confident about the reconstructed $\Delta_t C_{ant}^{anom}$ in the South Atlantic given our tests with synthetic data (*9*), we point out that such a shift in storage from the northern to the southern hemisphere was seen in previous $\Delta_t C_{ant}$ reconstructions, albeit based on a single meridional section (*30*).

A second set of major regions of anomalous change in inventory are the Indian and Pacific sectors of the Southern Ocean, where the changes in storage are about 20% lower than expected (Figure 3c). The tests with synthetic data showed that changes in these regions should be captured by the eMLR(C*) based reconstruction, although likely underestimated (*9*). We have some confidence in the robustness of this signal due to the fact that it is caused by a negative $\Delta_t C_{ant}^{anom}$ that is confined to the neutral density layers of Antarctic Intermediate Water and found in all ocean basins (Figure 4). We interpret this signal to be the result of the southward movement and strengthening of the westerly wind belt(*33*), which has caused large-scale coherent changes in the meridional overturning circulation in the Southern Ocean and the ventilation of the water masses (*34*, *35*). Further, the wind changes have caused increased upwelling over the Southern Ocean, and enhanced Ekman transport to the north, leading to shorter residence times of waters at the surface. This could have led to the weaker uptake and consequently weaker downward transport of anthropogenic CO_2 into the thermocline by the upper cell of the meridional overturning circulation, leading to the observed negative $\Delta_t C_{ant}^{anom}$ in the Antarctic Intermediate Water.

Additional support of our interpretation that the reconstructed $\Delta_t C_{ant}^{anom}$ are real stems from the overall agreement of our result with those inferred recently from a diagnostic ocean model(*21*). Although our changes are somewhat larger, the patterns agree well,

and support the conclusion that the changes primarily reflect changes in ocean circulation.

Implications

Our reconstructed changes in the oceanic inventory of anthropogenic CO_2 imply a continuing strong role of the ocean in the recent global carbon budget (Table 2). From 1994 to 2007, anthropogenic emissions added 111±8 Pg C to the atmosphere(*36*), most of which stemmed from the burning of fossil fuels (94±5 Pg C)(*5*). Of these emissions, 50±1 Pg C (46%) remained in the atmosphere(*37*). Our uptake estimate of 34±4 Pg C implies that the ocean accounts for the removal from the atmosphere of 31±4% of the total anthropogenic CO_2 emissions over this time period (Table 2). This anthropogenic CO_2 uptake fraction does not differ from that for the period from the preindustrial up to 1994(*1*).

Our ocean uptake estimate for anthropogenic CO_2 permits us also to provide a constraint on the net land uptake for the 1994 through 2007 period. This requires us to consider also the potential contribution of a small anomalous (non-steady-state) net flux of natural CO_2, emerging from processes such as ocean warming and climate variability-driven changes in ocean circulation and biology (*38*). We obtain a rough estimate of this contribution by using the surface ocean pCO_2 based air-sea flux estimate of (*39*) for the 1994 through 2007 period and subtracting from it the expected anthropogenic uptake flux consistent with (*17*), while accounting also for the steady-state outgassing of natural CO_2. This yields a cumulative anomalous net release of natural CO_2 of about 5±3 Pg C. The resulting net (natural and anthropogenic CO_2) ocean uptake estimate of 29±5 Pg C for the 1994 through 2007 period implies a net terrestrial biosphere sink over this period of 31±9 Pg, or about 2.4±0.7 Pg C yr^{-1} (Table 2). Our data-based net ocean uptake estimate confirms the model-based 26±4 Pg C ocean sink reported by the Global Carbon Project over the 1994 through 2007 period (*36*).

While the ~30% increase in the oceanic burden of anthropogenic CO_2 between 1994 and 2007 period constitutes a great service for humanity by slowing down the accumulation of CO_2 in the atmosphere, this service comes with the cost of increased ocean acidification(*40*). Our reconstructed increases in C_{ant} imply a deep reach of ocean acidification into the ocean's interior(*41*, *42*), causing a further shoaling of the ocean's saturation horizons for biogenic carbonate minerals(*43*), and a further squeezing of the available habitats for the organisms sensitive to changes in the ocean's CO_2 chemistry(*40*, *44*).

Documenting and quantifying these changes in anthropogenic CO_2 and ocean acidification requires the continuation of whole ocean observations of inorganic carbon and of the many ancillary variables needed to produce the internally consistent data products that are so crucial for analysing long-term changes in ocean carbon storage. In addition, the continuing documentation of the biogeochemical and physical changes in the ocean will be essential for understanding any forthcoming changes in ocean biology.

References:

1. C. L. Sabine *et al.*, The oceanic sink for anthropogenic CO_2. *Science (80-.).* **305**, 367–371 (2004).
2. B. I. McNeil, R. J. Matear, The non-steady state oceanic CO_2 signal: its importance, magnitude and a novel way to detect it. *Biogeosciences.* **10**, 2219–2228 (2013).
3. J. L. Sarmiento, J. C. Orr, U. Siegenthaler, A perturbation Simulation of CO_2 uptake in an Ocean General Circulation Model. *J. Geophys. Res.* **97**, 3621–3645 (1992).
4. R. A. Houghton, A. A. Nassikas, Global and regional fluxes of carbon from land use and land cover change 1850–2015. *Global Biogeochem. Cycles*. **31**, 456–472 (2017).
5. T. A. Boden, G. Marland, R. J. Andres, "Regional and National Fossil-Fuel CO_2 Emissions" (Oak Ridge; Tenn.; U.S.A, 2017), doi:10.3334/CDIAC/00001_V2017.
6. N. Gruber *et al.*, Oceanic sources, sinks, and transport of atmospheric CO_2. *Global Biogeochem. Cycles.* **23** (2009), doi:10.1029/2008GB003349.
7. L. D. Talley *et al.*, Changes in Ocean Heat, Carbon Content, and Ventilation: A Review of the First Decade of GO-SHIP Global Repeat Hydrography. *Ann. Rev. Mar. Sci.* **8**, 185–215 (2016).
8. A. Olsen *et al.*, The Global Ocean Data Analysis Project version 2 (GLODAPv2) – an internally consistent data product for the world ocean. *Earth Syst. Sci. Data*. **8**, 297–323 (2016).
9. D. Clement, N. Gruber, The eMLR(C*) Method to Determine Decadal Changes in the Global Ocean Storage of Anthropogenic CO_2. *Global Biogeochem. Cycles.* **32**, 654–679 (2018).
10. K. Friis, A. Körtzinger, J. Pätsch, D. W. R. Wallace, On the temporal increase of anthropogenic CO_2 in the subpolar North Atlantic. *Deep. Res. Part I.* **52**, 681–698 (2005).
11. J. L. Sarmiento, N. Gruber, *Ocean Biogeochemical Dynamics* (Princeton University Press, Princeton, New Jersey, 2006).
12. N. Gruber, Anthropogenic CO_2 in the Atlantic Ocean. *Global Biogeochem. Cycles.* **12**, 165–191 (1998).
13. S. Khatiwala *et al.*, Global ocean storage of anthropogenic carbon. *Biogeosciences.* **10**, 2169–2191 (2013).
14. T. DeVries, The oceanic anthropogenic CO_2 sink: Storage, air-sea fluxes, and transports over the industrial era. *Global Biogeochem. Cycles*. **28**, 631–647 (2014).
15. D. R. Jackett, T. J. McDougall, A Neutral Density Variable for the World's Oceans. *J. Phys. Oceanogr.* **27**, 237–263 (1997).
16. K. Hanawa, L. D. Talley, in *Ocean Circulation and Climate*, G. Siedler, J. Church, Eds. (Academic Press, San Diego, 2001), pp. 373–386.
17. S. E. Mikaloff Fletcher *et al.*, Inverse estimates of anthropogenic CO_2 uptake, transport, and storage by the ocean. *Global Biogeochem. Cycles.* **20**, 1–16 (2006).
18. L. Bopp, M. Lévy, L. Resplandy, J. B. Sallée, Pathways of anthropogenic carbon subduction in the global ocean. *Geophys. Res. Lett.* (2015), doi:10.1002/2015GL065073.
19. J. Marshall, K. Speer, Closure of the meridional overturning circulation through Southern Ocean upwelling. *Nat. Geosci.* **5**, 171–180 (2012).

20. M. Hoppema, W. Roether, R. G. J. Bellerby, H. J. W. de Baar, Direct measurements reveal insignificant storage of anthropogenic CO_2 in the Abyssal Weddell Sea. *Geophys. Res. Lett.* **28**, 1747–1750 (2001).

21. T. Devries, M. Holzer, F. Primeau, Recent increase in oceanic carbon uptake driven by weaker upper-ocean overturning. *Nature*. **542**, 215–218 (2017).

22. A. Olsen, A. M. Omar, E. Jeansson, L. G. Anderson, R. G. J. Bellerby, Nordic seas transit time distributions and anthropogenic CO_2. *J. Geophys. Res.* **115**, 1–14 (2010).

23. T. Tanhua *et al.*, Ventilation of the Arctic Ocean: Mean ages and inventories of anthropogenic CO_2 and CFC-11. *J. Geophys. Res.* **114**, 1–11 (2009).

24. A. Schneider, T. Tanhua, A. Körtzinger, D. W. R. Wallace, High anthropogenic carbon content in the eastern Mediterranean. *J. Geophys. Res.* **115**, C12050 (2010).

25. R. Wanninkhof *et al.*, Changes in deep-water CO_2 concentrations over the last several decades determined from discrete pCO_2 measurements. *Deep Sea Res. Part II.* **74**, 48–63 (2013).

26. S. Khatiwala, F. Primeau, T. Hall, Reconstruction of the history of anthropogenic CO_2 concentrations in the ocean. *Nature*. **462**, 346–349 (2009).

27. R. H. Gammon, J. Cline, D. Wisegarver, Chlorofluoromethanes in the Northeast Pacific Ocean: Measured vertical distributions and application as transient tracers of upper ocean mixing. *J. Geophys. Res.* **87**, 9441–9454 (1982).

28. T. Tanhua, A. Körtzinger, K. Friis, D. W. Waugh, D. W. R. Wallace, An estimate of anthropogenic CO_2 inventory from decadal changes in oceanic carbon content. *Proc. Natl. Acad. Sci.* **104**, 3037–3042 (2007).

29. R. Steinfeldt, M. Rhein, J. L. Bullister, T. Tanhua, Inventory changes in anthropogenic carbon from 1997–2003 in the Atlantic Ocean between 20°S and 65°N. *Global Biogeochem. Cycles*. **23**, 1–11 (2009).

30. R. Wanninkhof *et al.*, Detecting anthropogenic CO_2 changes in the interior Atlantic Ocean between 1989 and 2005. *J. Geophys. Res.* **115**, C11028 (2010).

31. F. F. Pérez *et al.*, Atlantic Ocean CO_2 uptake reduced by weakening of the meridional overturning circulation. *Nat. Geosci.* **6**, 146–152 (2013).

32. F. Fröb *et al.*, Irminger Sea deep convection injects oxygen and anthropogenic carbon to the ocean interior. *Nat. Commun.* **7**, 13244 (2016).

33. D. W. J. Thompson, S. Solomon, Interpretation of recent Southern Hemisphere climate change. *Science*. **296**, 895–899 (2002).

34. D. W. Waugh, F. Primeau, T. Devries, M. Holzer, Recent Changes in the Ventilation of the Southern Oceans. *Science (80-.).* **339**, 568–70 (2013).

35. T. Tanhua *et al.*, Temporal changes in ventilation and the carbonate system in the Atlantic sector of the Southern Ocean. *Deep. Res. Part II Top. Stud. Oceanogr.* **138**, 26–38 (2017).

36. C. Le Quéré *et al.*, Global Carbon Budget 2017. *Earth Syst. Sci. Data*. **10**, 405–448 (2018).

37. E. Dlugokencky, P. Tans, "Trends in atmospheric carbon dioxide" (Boulder, CO, USA, 2017), (available at http://www.esrl.noaa.gov/gmd/ccgg/tre).

38. R. F. Keeling, Comment on "The Ocean Sink for Anthropogenic CO_2." *Science (80-.).* **308**, 1743c–1743c (2005).

39. P. Landschützer, N. Gruber, D. C. E. Bakker, Decadal variations and trends of the global ocean carbon sink. *Global Biogeochem. Cycles*. **30**, 1–22 (2016).

40. S. C. Doney, V. J. Fabry, R. A. Feely, J. A. Kleypas, Ocean Acidification: The Other CO_2 Problem. *Ann. Rev. Mar. Sci.* **1**, 169–192 (2009).

41. R. A. Feely, Impact of Anthropogenic CO_2 on the $CaCO_3$ System in the Oceans. *Science (80-.).* **305**, 362–366 (2004).

42. F. F. Perez *et al.*, Meridional overturning circulation conveys fast acidification to the deep Atlantic Ocean. *Nature*. **554**, 515–518 (2018).

43. B. R. Carter *et al.*, Two decades of Pacific anthropogenic carbon storage and ocean acidification along Global Ocean Ship-based Hydrographic Investigations Program sections P16 and P02. *Global Biogeochem. Cycles*. **31**, 306–327 (2017).

44. K. J. Kroeker, R. L. Kordas, R. N. Crim, G. G. Singh, Meta-analysis reveals negative yet variable effects of ocean acidification on marine organisms. *Ecol. Lett.* **13**, 1419–1434 (2010).

45. N. Gruber, J. L. Sarmiento, T. F. Stocker, An improved method for detecting anthropogenic CO_2 in the oceans. *Global Biogeochem. Cycles*. **10**, 809–837 (1996).

46. P. Regnier *et al.*, Anthropogenic perturbation of the carbon fluxes from land to ocean. *Nat. Geosci.* **6**, 597–607 (2013).

47. C. Sabine, N. Gruber, Response to Comment on "The Ocean Sink for Anthropogenic CO_2." *Science (80-.).* **308**, 1743d–1743d (2005).

48. E. Hansis, S. J. Davis, J. Pongratz, Relevance of methodological choices for accounting of land use change carbon fluxes. *Global Biogeochem. Cycles*. **29**, 1230–1246 (2015).

49. R. M. Key *et al.*, A global ocean carbon climatology: Results from Global Data Analysis Project (GLODAP). *Global Biogeochem. Cycles*. **18** (2004), doi:10.1029/2004GB002247.

50. T. Tanhua *et al.*, Atlantic Ocean CARINA data : overview and salinity adjustments. *Earth Syst. Sci. Data*, 17–34 (2010).

51. R. M. Key *et al.*, The CARINA data synthesis project: introduction and overview. *Earth Syst. Sci. Data*. **2**, 105–121 (2010).

52. K. Suzuki, T., Ishii, M., Aoyama, A., Christian, J. R., Enyo, L. A. Kawano, T., Key, R. M., Kosugi, N., Kozyr, A., Miller, S. Murata, A., Nakano, T., Ono, T., Saino, T., Sasaki, K., C. L. D., Takatani, Y., Wakita, M., and Sabine, "PACIFICA Data Synthesis Project" (2013), doi:10.3334/CDIAC/OTG.PACIFICA_NDP092.

53. S. K. Lauvset *et al.*, A new global interior ocean mapped climatology: The 1°x1° GLODAP version 2. *Earth Syst. Sci. Data*. **8**, 325–340 (2016).

54. R. A. Locarnini *et al.*, "World Ocean Atlas 2013, Volume 1: Temperature" (2013).

55. M. M. Weng *et al.*, "World Ocean Atlas 2013: Volume 2: Salinity" (2013).

56. M. AOYAMA *et al.*, Current Status of Homogeneity and Stability of the Reference Materials for Nutrients in Seawater. *Anal. Sci.* **28**, 911–916 (2012).

57. R. E. Sonnerup, P. D. Quay, A. P. McNichol, The Indian Ocean ^{13}C Suess Effect. *Global Biogeochem. Cycles*. **14**, 903–916 (2000).

58. Y. Plancherel, K. B. Rodgers, R. M. Key, a. R. Jacobson, J. L. Sarmiento, An assessment of regression methods used to measure changes in the oceanic distribution of anthropogenic carbon. *Biogeosciences*. **10**, 4801–4831 (2013).

59. N. Gruber, J. L. Sarmiento, in *THE SEA: Biological-Physical Interactions in the Oceans*, A. R. Robinson, J. J. McCarthy, B. J. Rothschild, Eds. (John Wiley and Sons, New York, 2002), vol. 12, pp. 337–399.

60. A. C. Martiny *et al.*, Strong latitudinal patterns in the elemental ratios of marine plankton and organic matter. *Nat. Geosci.* **6**, 279–283 (2013).

61. R. J. Woosley, F. J. Millero, R. Wanninkhof, Rapid anthropogenic changes in CO_2 and pH in the Atlantic Ocean: 2003-2014. *Global Biogeochem. Cycles*. **30**, 70–90 (2016).

62. W. S. Broecker, S. Blanton, W. M. Smethie, G. Ostlund, Radiocarbon decay and oxygen utilization in the deep Atlantic Ocean. *Glob. Biogeochem. Cycles*. **5**, 87–117 (1991).

63. B. I. McNeil, R. J. Matear, R. M. Key, J. L. Bullister, J. L. Sarmiento, Anthropogenic CO_2 Uptake by the Ocean Based on the Global Chlorofluorocarbon Data Set. *Science (80-.).* **299**, 235–239 (2003).

64. S. van Heuven, D. Pierrot, J. W. B. Rae, E. Lewis, D. W. R. Wallace, CO2sys: MATLAB Program Developed for CO_2 System Calculations. (2011), , doi:10.3334/CDIAC/otg.CO2SYS_MATLAB_v1.1.

65. C. Mehrbach, C. H. Culberson, J. E. Hawley, R. M. Pytkowicz, Measurement of the apparent dissociation constants of carbonic acid in seawater at atmospheric pressure. *Limnol. Ocean.* **18**, 897–907 (1973).

66. A. G. Dickson, F. J. Millero, A comparison of the equilibrium constants for the dissociation of carbonic acid in seawater media. *Deep Sea Res.* **34**, 1733–1743 (1987).

67. S. Kouketsu, A. M. Murata, Detecting decadal scale increases in anthropogenic CO_2 in the ocean. *Geophys. Res. Lett.* **41**, 4594–4600 (2014).

68. J. L. Sarmiento, C. LeQuéré, S. W. Pacala, Limiting future atmospheric carbon dioxide. *Glob. Biogeochem. Cycles*. **9**, 121–137 (1995).

69. K. Matsumoto, N. Gruber, How accurate is the estimation of anthropogenic carbon in the ocean? An evaluation of the ΔC* method. *Global Biogeochem. Cycles*. **19** (2005), doi:10.1029/2004GB002397.

70. L. Resplandy *et al.*, Revision of global carbon fluxes based on a reassessment of oceanic and riverine carbon transport. *Nat. Geosci.* **11** (2018), doi:10.1038/s41561-018-0151-3.

71. A. R. Jacobson, S. E. Mikaloff Fletcher, N. Gruber, J. L. Sarmiento, M. Gloor, A joint atmosphere-ocean inversion for surface fluxes of carbon dioxide: 1. Methods and global-scale fluxes. *Global Biogeochem. Cycles*. **21**, 1–13 (2007).

432

Acknowledgments:

We are deeply indebted to the large number of principal investigators, scientists and technicians that acquired the high-quality oceanographic data that made our study possible. This global synthesis is the outcome of an effort led by the joint IMBER-SOLAS Ocean carbon cycle working group 2. We acknowledge the support from the two parent organizations IMBER and SOLAS. We also thank for the insightful and supportive input by the reviewers. **Funding**: We are grateful to the many funding agencies in the various countries that financially supported the global ship-based surveys that underpin much of this work. In particular, we would like to acknowledge the funding from the U.S. National Science Foundation and from the National Oceanic and Atmospheric Administration (NOAA), and the GO-SHIP program together with the International ocean carbon coordination project (IOCCP) for their efforts to initiate and coordinate the repeat hydrography program. The work of NG and DC was supported by ETH and the FP7 projects CarboChange (264879) and Geocarbon (283080). SvH also received support by CarboChange (264879). RW, RAF, and BRC acknowledge support of Oceanic and Atmospheric Research NOAA, U.S. Department of Commerce, including resources from the NOAA Global Ocean Monitoring and Observations Division (fund reference 100007298). This is contribution number 4796 from the NOAA Pacific Marine Environmental Laboratory and JISAO contribution 2018-0185. MI acknowledges support from Japan Meteorological Agency and MEXT KAKENHI Grant Number 24121003 “NEOPS” and JP16H01594 “OMIX”. SKL acknowledges support from the Research Council of Norway (214513). FFP was supported by Ministerio de Economía y Competitividad through the ARIOS (CTM2016-76146-C3-1-R) project co-funded by the Fondo Europeo de Desarrollo Regional 2014-2020 (FEDER) and EU Horizon 2020 through the AtlantOS project (grant agreement 633211). **Author contributions:** NG led the global synthesis project together with RW, RAF, TT, MI, JM. NG conceived and developed the eMLR(C*) method together with DC, analyzed the results, and wrote the paper with input by all co-authors. DC undertook additional quality controls on the data with input by SvH, conducted the estimation of the changes in anthropogenic

463 CO_2 together with NG, and supported all analyses. SvH performed additional
464 inversion of the data. AO led the team that conducted the secondary quality control of
465 the GO-SHIP and JGOFS/WOC-era cruises. All authors provided their expertise at all
466 stages, were involved in the analysis and interpretation of the data, and contributed to
467 the writing of the manuscript. **Competing interests**: The authors declare that they
468 have no competing interests. **Data and materials availability:** The inorganic carbon
469 observations from GLODAPv2 underlying this study are available from the GLODAP
470 website: www.glodap.info. The anthropogenic CO_2 estimates reported in this paper
471 can be obtained through NCEI's Ocean Carbon Data System:
472 www.nodc.noaa.gov/ocads/index.html.
473
474
475

476 **Supplementary Materials**

477 Supplementary Text
478 Figs. S1 to S10
479 Tables S1 to S3
480 References (49)-(71)
481
482

Figures

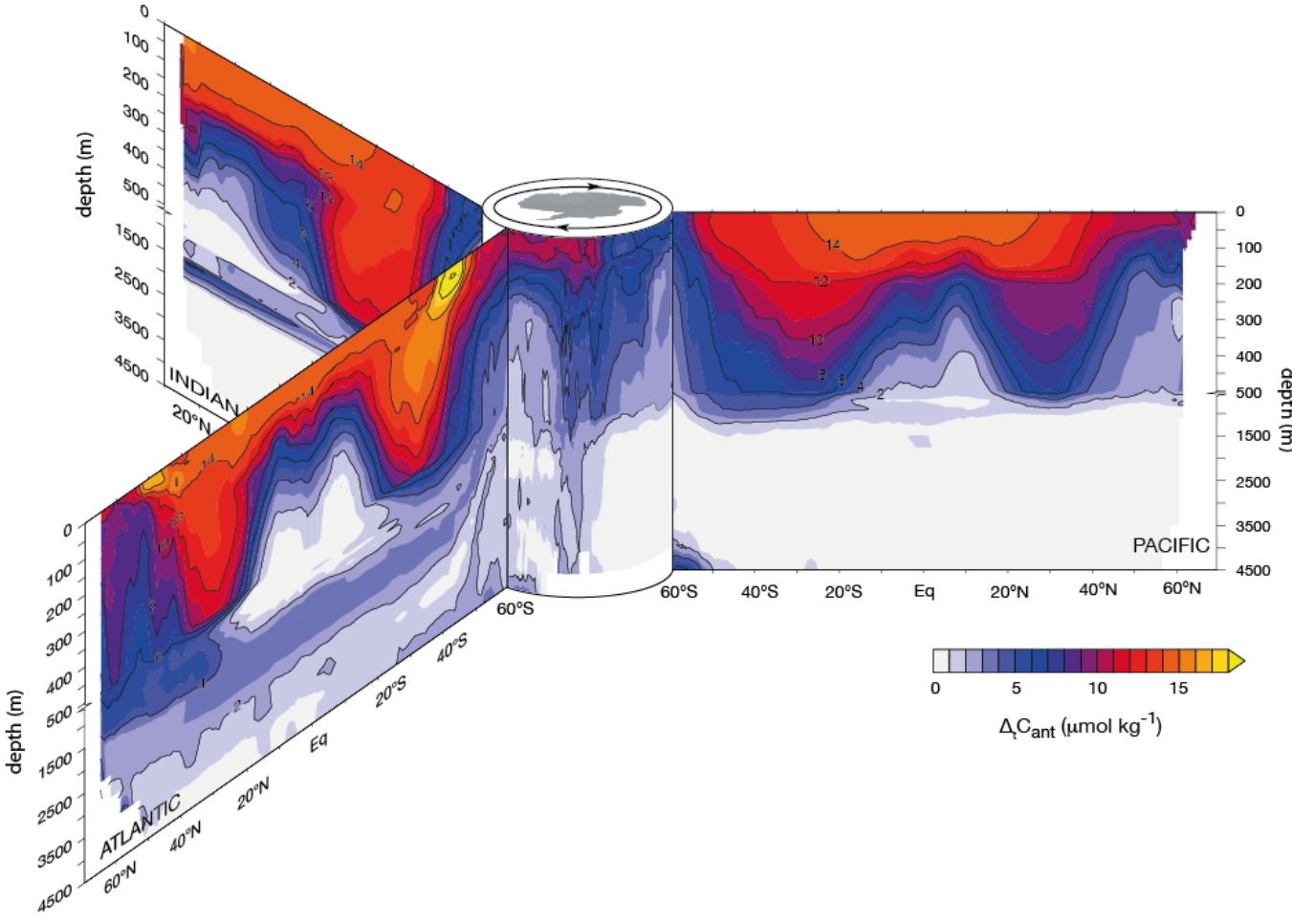

Figure 1: Vertical sections of the change in C_{ant}, $\Delta_t C_{ant}$, between the JGOFS/WOCE era (~1994) and the Repeat Hydrography/GO-SHIP era (~2007). Shown are the zonal mean sections in each ocean basin organized around the Southern Ocean in the center. The upper 500 m are expanded. Contour intervals are 2 µmol kg^{-1}.

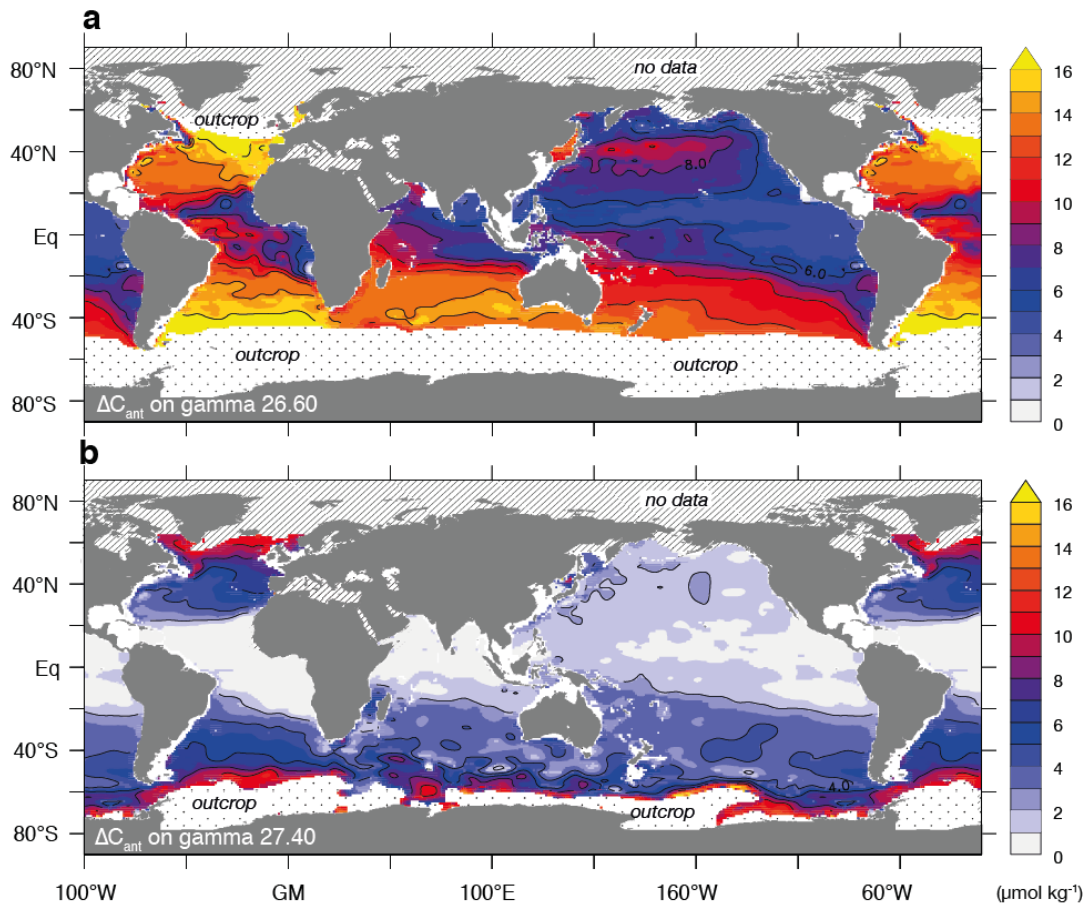

493

494 **Figure 2:** Distribution of the change in anthropogenic CO_2, $\Delta_t C_{ant}$, between 1994 and
495 2007 on two selected neutral surfaces. (a) $\Delta_t C_{ant}$ on the neutral surface 26.60 kg m^{-3},
496 representing subtropical mode waters and located around 400 m depth in the centers
497 of the subtropical gyres. (b) $\Delta_t C_{ant}$ on the neutral surface 27.40 located at a depth of
498 about 1000 m. In the southern hemisphere and in the Indian and Pacific oceans, this
499 neutral surface represents southern-sourced Antarctic Intermediate Water, while in the
500 North Atlantic it represents Intermediate Water formed in the north. Stippled areas
501 poleward of the highest concentration of $\Delta_t C_{ant}$ indicate the outcrop areas of these
502 neutral surfaces. Hatched areas indicate regions where no estimate of $\Delta_t C_{ant}$ was
503 possible due to data limitations.

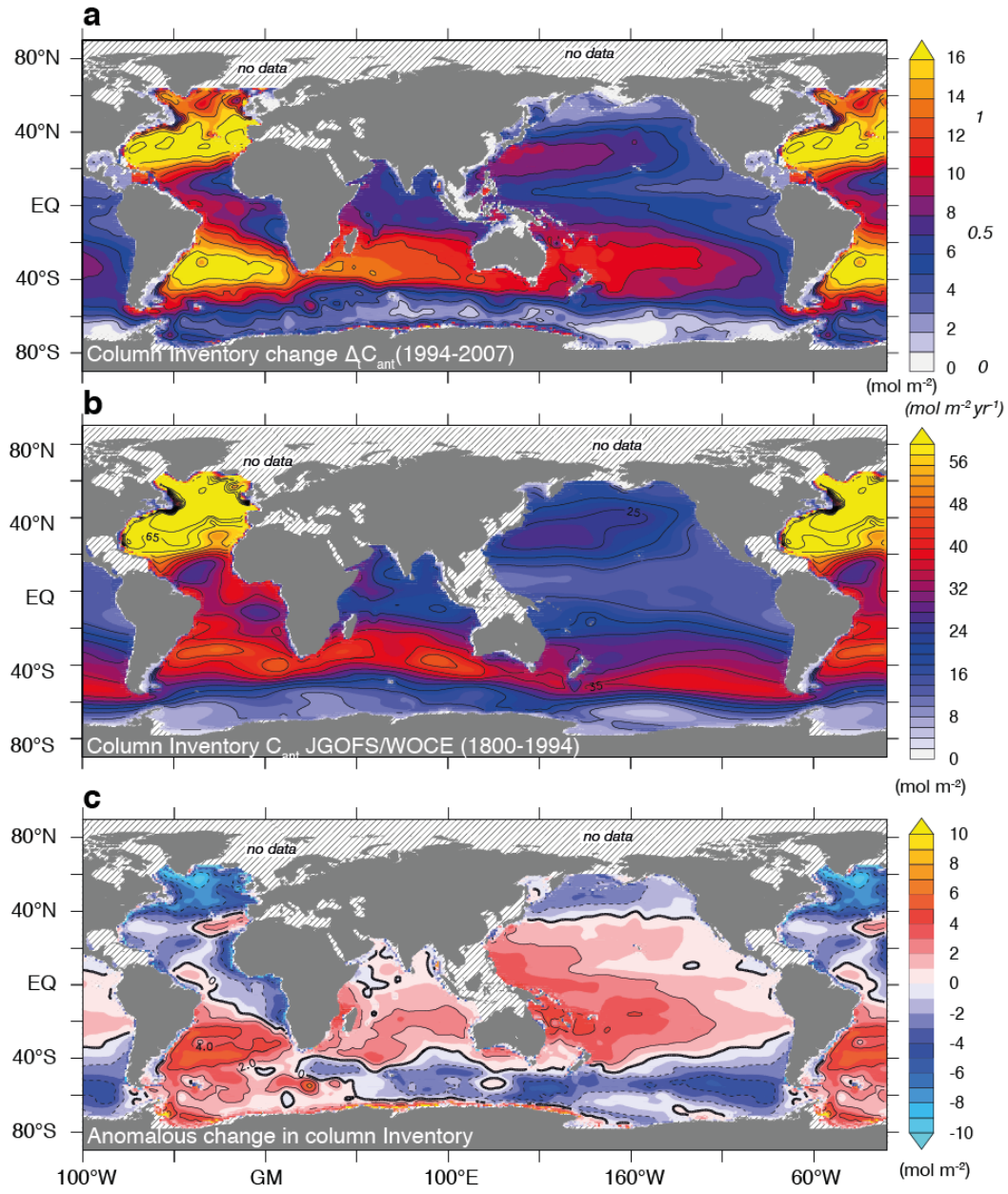

Figure 3: Maps of the column inventories of anthropogenic CO_2 in the ocean (0-3000m). (a) Change in column inventory between 1994 and 2007 based on the eMLR(C*) method. (b) Column inventory for the year 1994 (*1*) based on the ΔC* method(*45*). (c) Anomalous change in column inventory estimated from the difference between the change in the vertical column inventory (shown in a) and that expected on the basis of the transient steady-state model and the C_{ant} inventory shown in (b), namely $\Delta_t C_{ant}^{anom} = \Delta_t C_{ant} - \alpha \cdot C_{ant}(1994)$, $\alpha = 0.28$. The column inventories were obtained by vertically integrating the values from the surface down to 3000 m.

Hatched areas indicate regions where no estimate of $\Delta_t C_{ant}$ was possible due to data limitations.

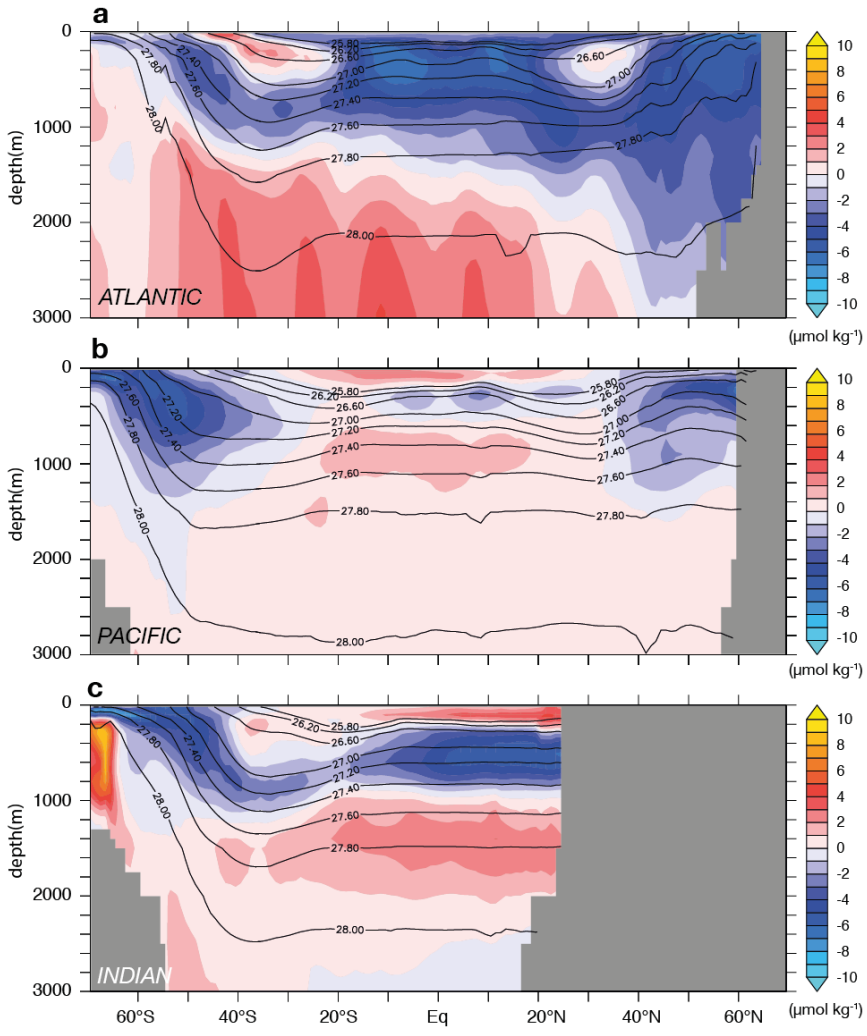

Figure 4: Zonal mean sections of the anomalous change in C_{ant}, i.e., $\Delta_t C_{ant}^{anom} = \Delta_t C_{ant} - \alpha \cdot C_{ant}(1994)$, $\alpha = 0.28$. (a) Zonal mean section in the Atlantic, (b) as (a) but for the Pacific, and (c), as (a) but for the Indian Ocean. Selected isolines of zonally averaged neutral density are shown as contour lines in all plots.

523 **Tables**

524 *Table 1:* Change in the inventory of anthropogenic CO_2 between 1994-2007 as
525 estimated on the basis of the eMLR(C*) method. Shown in italics are the estimated
526 uncertainty based on the sensitivity and Monte Carlo analyses.
527

	Atlantic (Pg C)	Pacific (Pg C)	Indian (Pg C)	Other basins‡ (Pg C)	Global (Pg C)
Northern hemisphere	6.0 ±*0.4*†	5.2 ±*0.6*	0.8 ±*0.4*	1.5 ±*0.6*	13.5 ±*1.0*
Southern hemisphere	5.9 ±*1.2*†	8.0 ±*1.2*	6.3 ±*3.4*	~0	20.1 ±*3.8*
Entire basin	11.9 ±*1.3*	13.2 ±*1.3*	7.1 ±*3.4*	1.5 ±*0.6*	**33.7 ±*4.0***

528 †includes an estimated 1 Pg C to account for the accumulation below 3000 m, with 0.7 Pg C allocated
529 to the North Atlantic, and 0.3 Pg C to the South Atlantic (see main text)
530 ‡estimated storage in the Arctic and Mediterranean Sea (see supplementary material)
531
532
533

534 *Table 2*: Global Budget for CO_2 for both the period 1800 until 1994, and the decadal
535 period from 1994 until 2007. In comparison to previous budgets (*1*), we include now
536 explicitly also the potential loss of natural CO_2 from the ocean as a component of the
537 budget. Note that the potential contribution of changes in the land to ocean carbon
538 fluxes through aquatic systems(*46*) is not considered here.

CO_2 sources and sinks	1800 to 1994 (Pg C) (a)	1994 to 2007 (Pg C) (b)
Constrained sources and sinks		
(1) Emissions of C_{ant} from fossil fuel and cement production	244±20	94±5 (c)
(2) Increase of CO_2 in the atmosphere	-165±4	-50±1 (d)
(3a) Uptake of C_{ant} by the ocean	**-118±19**	**-34± 4(e)**
(3b) Loss of natural CO_2 by the ocean	7 ± 10(f)	5±3 (g)
(3) Net ocean CO_2 uptake	-111±21	-29±5
Inferred terrestrial balance		
(4) Net terrestrial balance [-(1) -(2) -(3)]	32 ± 30	-15±7
Terrestrial balance		
(5) Emissions of C_{ant} from land use change	100 to 180	16±6(h)
(6) Terrestrial biosphere sink [-(1)-(2)-(3)] -(5)	-68 to -148	-31±9

539 (a) budget as listed in Sabine et al. (2004), except for 3b (ref (*1*))
540 (b) the numbers correspond to the period from mid 1994 to mid 2007.
541 (c) Boden, Marland and Andres (2017) (ref (*5*))
542 (d) Dlugokencky and Tans (2017) (ref (*37*))
543 (e) this study
544 (f) Keeling (2005), Sabine and Gruber (2005) (refs (*38*, *47*)
545 (g) see text, based on Landschützer et al. (2016) (*39*)
546 (h) average of Houghton and Nassikas (2017) and Hansis et al. (2015) (refs (*4*, *48*))
547

Supplementary Materials for

The oceanic sink for anthropogenic CO_2 from 1994 to 2007

Nicolas Gruber, Dominic Clement, Brendan R. Carter, Richard A. Feely, Steven van Heuven, Mario Hoppema, Masao Ishii, Robert M. Key, Alex Kozyr, Siv K. Lauvset, Claire Lo Monaco, Jeremy T. Mathis, Akihiko Murata, Are Olsen, Fiz F. Perez, Christopher L. Sabine, Toste Tanhua, and Rik Wanninkhof

correspondence to: nicolas.gruber@env.ethz.ch

This PDF file includes:

Materials and Methods

Data

The main data we employ come from the merged and internally consistent GLODAPv2 data product(*8*), which consists of high-quality measurements of dissolved inorganic carbon (*DIC*), total alkalinity (*Alk*), and related parameters, such as the macronutrients nitrate, phosphate, and silicic acid, and dissolved oxygen, from a total of 724 cruises covering the global ocean and spanning the period from 1972 through 2012. This global data product was built on the basis of earlier collections, starting with the first version of GLODAP(*49*), but also including the CARINA collection in the Atlantic and Southern Ocean(*50*, *51*) and the PACIFICA collection in the Pacific(*52*). Numerous additional cruises with high quality data, particularly from the Repeat Hydrography /GO-SHIP program(*7*) were included into GLODAPv2 as well, making this the world's largest and most complete collection of interior ocean inorganic carbon data(*8*). The GLODAPv2 data underwent strict quality control procedures (i.e., bias adjustments) in order to achieve internal consistency, which is a key requirement for the analysis of long-term trends. The level of consistency of the data obtained after adjustments was determined to be better than 0.005 in salinity (S), 1% in oxygen (O_2), 2% in nitrate (NO_3^-), 2% in silicic acid ($Si(OH)_4$), 2% in phosphate (PO_4^{3-}), 4 μmol kg^{-1} in dissolved inorganic carbon (DIC), and 6 μmol kg^{-1} in total alkalinity (*Alk*).

We modified the GLODAPv2 data product in two ways. First, we added two GO-SHIP cruises in the Atlantic (A16S, 2013/2014, and A16N, 2013, https://cchdo.ucsd.edu/cruise/33RO20131223, 33RO20130803) in order to have a better temporal coverage of this basin for the Repeat Hydrography Program/GO-SHIP era (henceforth referred to as GO-SHIP era, although this era is ongoing). Second, several cruises/stations were excluded from the analyses for a number of reasons: (i) too early, i.e., all data before 1981 were excluded in order to avoid the inclusion of data with possibly enhanced measurement uncertainty and also data that require an excessive temporal adjustment, (ii) outside analysis domain, i.e., data stemming from marginal seas (Mediterranean, Sea of Japan, etc.) and north of 65°N were not considered, and (iii) not all variables needed to compute C* and to establish the linear regressions were available. The third criterion, i.e., the availability of the whole suite of variables was by far the most important exclusion criterion, as it excluded about 75% of all samples in GLODAPv2. A final manual quality control (iv) checked for stations with an excessive amount of scatter in the computed C* tracer. This affected mostly a few selected stations, primarily located in the Southern Hemisphere (Figure S1).

Given our goal to estimate decadal changes in anthropogenic carbon between the 1990s (JGOFS/WOCE era) and the 2000s and 2010s (GO-SHIP era), we assigned each cruise to one of these two eras, using January 1st, 2000 as the separation. Figure S1 depicts the resulting spatial distribution of the cruises for each of the two eras, color-coded according to the year of observation. In Figure S2, the data distribution in time is shown, color coded according to ocean basin. The overall distribution is relatively homogeneous, with the median year for all retained measurements being 1994 for the JGOFS/WOCE era and 2007 for the GO-SHIP era. Unfortunately, there are also large spatial gaps. Especially striking is the relatively poor coverage of the Indian Ocean during the GO-SHIP era up to 2012.

In order to map the estimated change in anthropogenic CO_2 to the global ocean, we employ two gridded products, i.e., the gridded GLODAPv2 product(*53*) for nitrate, phosphate, silicic acid, oxygen, and the apparent oxygen utilization ($AOU = O_2^{sat} - O_2$), and the gridded World Ocean Atlas 2013 (WOA) product for temperature(*54*) and salinity(*55*). Although the GLODAPv2 gridded product is based on fewer data than the WOA product, its source data is fully quality controlled and internally consistent. In contrast, the WOA product may have inherited substantial biases from its source data, which have been subject to only a minimum level of 2nd quality control. This is a particular concern for the nutrients since standard reference materials for these parameters that would allow for a more direct comparability of the different measurements have become available only very recently(*56*). An additional reason to employ the GLODAPv2 product is that it is consistent with the data that was used to determine the predictive relationships for $\Delta_t C_{ant}$. This avoids mapping biases, particularly in the deeper parts of the ocean, where small offsets can lead to substantial errors in the estimation of $\Delta_t C_{ant.}$ Since quality issues and biases are much smaller for S and T, owing to their high inherent accuracy and the well-established use of standards, we opted for the WOA product for these two parameters. In the sensitivity studies described in more detail below, we explore the impact of this data selection choice.

Determination of change in anthropogenic CO_2:

We determine the change in the oceanic anthropogenic CO_2 concentration between the two eras by employing the recently developed eMLR(C*) method(*9*). This method builds on the well-established eMLR method(*10*, *57*), but extends it in several ways to deal primarily with (i) the temporal inhomogeneity of the data and (ii) with the spatial inhomogeneity of the observations, i.e., the fact that only a subset of the cruises represent repeat occupations of the same lines. The eMLR(C*) method employs a probabilistic approach in the selection of the independent variables for the eMLR, thereby avoiding many of the problems associated with the choice of variables when building regression models(*43*, *58*). A full description of the method including a detailed assessment of its performance on the basis of synthetic data from a hindcast simulation with an ocean biogeochemical model is given in ref (*9*). Here, we provide a brief description including the specific modifications undertaken to deal with real observations.

The method proceeds in three steps (Figure S3). In the first step, the semi-conservative tracer $C^* = DIC - r_{C:P}\ PO_4^{3-} - 1/2\ (Alk + r_{N:P}\ PO_4^{3-})$ (*45*, *59*) is computed from the measured *DIC*, *Alk* and phosphate (PO_4^{3-}) assuming a constant stoichiometric C:P and N:P ratio during photosynthesis and respiration/remineralization ($r_{C:P}$ = 116:1, $r_{N:P}$ = 16:1). We use here phosphate instead of nitrate in order to avoid issues with denitrification (*59*), even though the relative measurement precision is better for nitrate than for phosphate. If the assumption of constant stoichiometric ratios is correct, then the spatio-temporal distribution of C* reflects only the effect of the exchange of natural and anthropogenic CO_2 across the air-sea interface on the observed DIC(*6*). This strongly enhances the interpretability of the signals - an advantage that largely persists even when considering the fact that the stoichiometric ratios $r_{C:P}$ and $r_{N:P}$ are likely variable(*60*). A corollary advantage of using *C** in the eMLR method compared to the commonly used *DIC*(*30*, *43*, *61*) is the smaller variance in *C**, permitting us to develop more accurate statistical models(*9*).

In the second step, the C^* values for each observational era are normalized to the median for the respective periods (1994 for JGOFS/WOCE and 2007 for GO-SHIP). This normalization is achieved by assuming a transient steady state(*27*), which applies strictly for linear systems that are exponentially forced for an amount of time that is longer than the adjustment time– a condition that is largely met by the ocean carbon uptake(*28*) (see below for a more thorough discussion). This assumption predicts that in an ocean with time-constant circulation and mixing, the change in anthropogenic CO_2 burden between two years is proportional to the amount of anthropogenic CO_2 that is already present, with the proportionality determined by the relative change in atmospheric CO_2 between these two years(*28*), i.e., $C^*(t^{ref}) = C^*(t) - \beta(t) \cdot C_{ant}(t^{ref})$, with $\beta(t) = (CO_2^{atm}(t) - CO_2^{atm}(t^{ref}))/(CO_2^{atm}(t^{ref}) - CO_2^{atm}(t^{pi}))$[1], where t^{ref} is the reference year, t^{pi} is the preindustrial time and t is the year the measurement was taken. We use the global mean atmospheric CO_2 from ref (*37*) for CO_2^{atm} at times t and t^{ref}, and a value of 280 ppmv for atmospheric CO_2 at preindustrial time, i.e., $CO_2^{atm}(t^{pi})$. For the JGOFS/WOCE period, t_1^{ref}, we use for $C_{ant}(t_1^{ref})$ the globally gridded estimate of Sabine et al.(*49*). For the GO-SHIP period, t_2^{ref}, we constructed a corresponding distribution for $C_{ant}(t_2^{ref})$ from $C_{ant}(t_1^{ref})$ using the same transient steady state assumption, i.e., we scaled up the estimates for 1994 to 2007 using α=0.28 (see below for detailed justification). Since the majority of the measurements were taken relatively close in time to the two reference years, these adjustments are usually less than 2 to 3 µmol kg^{-1}. As a result, the sensitivity of the final results to these choices is very small (see ref (*9*)).

In the third step, the adjusted data from the two observational eras are fitted with multiple linear regressions. To this end, we binned the data into ranges of neutral density, i.e., isoneutral slabs: 14 for the Atlantic and 12 for the combined Indo-Pacific ocean basins (Table S1). Data above 150 m were excluded from the fit in order to avoid the inclusion of seasonal biases. The C^* observations for each of the 26 slabs from the JGOFS/WOCE period (t_1^{ref}) were then fitted with linear functions of the form: $C^*(t_1^{ref}) = a_{1,0} + \sum a_{1,i} \cdot T_i(t_1) + residual(t_1)$, where $a_{1,0}$ and $a_{1,i}$ are the coefficients of the linear fit, $T_i(t_1)$ are the i independent, co-measured variables used as predictors. The same procedure was completed for the data from the GO-SHIP period (t_2^{ref}), i.e., $C^*(t_2^{ref}) = a_{2,0} + \sum a_{2,i} \cdot T_i(t_2) + residual(t_2)$. The coefficients of the two fits are then combined to form the eMLR-based estimate of the change in anthropogenic CO_2 between the two reference periods, i.e., $\Delta C_{ant}(t_2^{ref}-t_1^{ref}) = (a_{2,0} - a_{1,0}) + \sum (a_{2,i}-a_{1,i}) \cdot T_i^{clim}$, where T_i^{clim} is the climatological distribution of the independent tracer T_i. We use a probabilistic approach in our selection of the independent variables (see also ref (*43*)). For each isoneutral slab and ocean basin, we first fit all possible combinations of the following 7 independent variables: temperature, salinity, phosphate, silicic acid, $PO_4^* = PO_4 - 16 \cdot NO_3 + 2.9$(*62*), oxygen, and *AOU* under the constraint that a minimum of two, but not more than 5 independent tracers are selected. This gives a total of 112 combinations. Out of these combinations, the 10 best fits are selected for each subset, with the quality of the fit determined from the combined root mean square error (RMSE) of both survey periods. Each of these 10 best fits are then combined with the climatological fields of the independent tracers T_i^{clim}, to estimate the change in anthropogenic CO_2 throughout the global ocean.

[1] Please note that the corresponding equation (6) in ref(*9*) is missing the $CO_2^{atm}(t^{pi})$ term in denominator. This is a mistake and a correction will be submitted to the journal.

We employ two methods to estimate the change in the anthropogenic CO_2 in the top 150 m. For waters with a neutral density higher than 26.0 kg m^{-3}, i.e., for the isoneutral slabs outcropping at temperate latitudes and higher, we extrapolate the eMLR equations from the ocean interior of that slab all the way to the surface. For the lower densities, we employ the transient equilibrium approach(*63*), i.e., we make the well-tested assumption that the CO_2 system in these waters has followed the increase in atmospheric CO_2 closely(*11*). This permits us to compute the change in anthropogenic CO_2 directly from the change in atmospheric CO_2 using thermodynamic considerations only. Specifically, we use eq 10.2.16 in ref (*11*) to estimate the change in anthropogenic CO_2 in the upper ocean by computing $\Delta_t C_{ant}^{eq}(t_2^{ref} - t_1^{ref}) = 1/\gamma \cdot DIC/pCO_2 \cdot (pCO_2^{atm}(t_2^{ref}) - pCO_2^{atm}(t_1^{ref}))$, where *DIC* and pCO_2 are the in situ values, where γ is the buffer (Revelle) factor and where we evaluated the right-hand side using CO2SYS(*64*) employing the Mehrbach constants(*65*) as refitted by Dickson and Millero(*66*) using the climatological values for temperature, salinity, *DIC* and *Alk*.

Calculations of changes in the column inventory of anthropogenic CO_2:

To compute the changes in the column inventory of anthropogenic CO_2, any negative values are set to zero and the resulting non-negative values are then integrated from the surface down to 3000 m. We do not integrate to greater depth, as we consider the reconstruction to be too uncertain there. In addition, we expect only a very small fraction of the total increase in the oceanic burden of anthropogenic CO_2 to accumulate below 3000 m since model simulations, as well as the total anthropogenic CO_2 burden from the pre-industrial to the 1994 (*1*), suggest that this fraction is substantially less than 5%. Nevertheless, we added 1 Pg C to the inventory of the Atlantic (0.7 Pg C in the North Atlantic, and the remaining 0.3 Pg C in the South Atlantic) to account for the contribution of the waters below 3000 m. This number as well as its distribution is largely based on the fraction of uptake into these waters that occurred between the preindustrial and 1994(*1*).

We also take into account the increase in anthropogenic CO_2 in regions not covered by our method, i.e., the Arctic, the Nordic Seas (north of 65°N) and the Mediterranean. (Note that our estimate covers the other marginal seas, namely the Caribbean, the Gulf of Mexico, and the Sea of Japan). To account for the contribution of these unmapped regions, we use independent estimates of the anthropogenic CO_2 accumulation in these regions. The majority of these estimates concern the total inventory, making it necessary to scale them to the time period of interest here, i.e., 1994 through 2007. To this end, we apply again the transient steady state assumption, and scale the inventories with a scaling factor α=0.28 (see below). We also use this assumption to correct the reported inventories back to the same starting year, i.e., 1994. This yields, for the Arctic, starting from the reported range of inventory of between 2.5 to 3.3 Pg C for 2005(*23*) an expected change of 0.6 to 0.9 Pg C between 1994 and 2007. For the Nordic Seas, we infer an increase of 0.2 to 0.4 Pg C, based on an inventory estimate of 0.9 to 1.4 Pg for 2002(*22*). For the Mediterranean, the corresponding estimate is 0.3 to 0.6 Pg C, computed from the reported inventory of 1.3 to 2.1 Pg C for 2001(*24*). In total, we estimate that we need to add between 1.2 and 1.9 Pg C (central estimate: 1.5 Pg C) to our mapped estimate to obtain the global change in the oceanic inventory of anthropogenic CO_2 between 1994 and 2007.

Uncertainties:

Using synthetic data from a hindcast simulation with the NCAR CCSM model, Clement and Gruber (*9*) investigated in detail the major sources of errors and uncertainties in the reconstructed $\Delta_t C_{ant}$ fields. While the eMLR(C*) method was found to perform very well with a near zero global bias, some persistent biases were found at the basin-scale and sub-basin scale level. The tests with the model revealed that the major cause for these biases are changes in ocean circulation whose impact on the accumulation on C_{ant} are not fully captured by the eMLR(C*) method (*9*). In contrast, the very skewed sampling in time and space, the assumption about transient steady state, and many other challenges mattered much less. These biases induced by circulation variability need to be taken carefully into account when interpreting the anomalous changes in $\Delta_t C_{ant}$.

To assign uncertainties to our reconstructed $\Delta_t C_{ant}$, we use two complementary approaches, each of which addresses a different aspect of uncertainty. The first approach attempts to propagate the uncertainties associated with the variable selection for the multiple linear regression models forward to the final estimated change in anthropogenic CO_2. This addresses one of the most important contributions to random uncertainty within the approach (cf. (*9*)). To this end, we employ a Monte Carlo method, where we select for each realization one member randomly from the 10 best regression models for each subsettted region and isoneutral slab and estimate the change in anthropogenic CO_2 for that model set. This procedure is repeated 100 times, yielding 100 spatial distributions of the change in anthropogenic CO_2 across the global ocean. We then use the standard deviation of these estimates as a measure of the random uncertainty.

In the second approach, we attempt to assess the potential impact on $\Delta_t C_{ant}$ of the subjective choices in the estimation procedure on the reconstructed change in anthropogenic CO_2. To this end, we used an ensemble of sensitivity analyses, wherein we made alternative choices along the three-step procedure visualized in Figure S3. Specifically, we altered (i) the climatological data the eMLR coefficients were applied on to estimate $\Delta_t C_{ant}$ globally (V102), (ii) the set of variables used to fit C^* (V103 and 106), (iii) the number and distribution of regions used to subset the data (V104, V105, V107), (iv) the number of isoneutral slabs considered in the vertical subsetting (V109 and V110), (v) the data employed to determine C^* (V108: no A16 cruise, and V114: all GLODAPv2 data used, i.e., no application of the exclusion criteria described above), (vi) how $\Delta_t C_{ant}$ is estimated in the upper 150 m of the water column (V111 and V112), and (vii) how C^* is defined (V113). Table S2 provides a detailed description of the standard estimate (V101) and of the 13 sensitivity cases considered. We use the interquartile range (IQR) of the 14 cases as an estimate of the systematic uncertainty associated with the reconstructed change in anthropogenic CO_2.

Table S3 lists the reconstructed changes in anthropogenic CO_2 between 1994 and 2007 for the standard case as well as for each of the 13 sensitivity cases. The median column inventories differ little from the "best" estimate provided by the standard case. Figure S4 shows the corresponding column inventories and Figure S5 the contribution of the different ocean basins to the global total.

The final uncertainty in inventory is estimated by taking the square root of the sum of squared uncertainties from both the Monte Carlo and the ensemble-based estimates, where we multiplied in both cases the uncertainties first by two, i.e., we used twice the

IQR and twice the standard deviation to allow for unrecognized uncertainties. For all regions, the total uncertainty is dominated by the uncertainty stemming from the ensembles, while the contribution of the Monte Carlo based estimates is rather small.

Supplementary Text

Comparison with regional estimates:

The eMLR(C*)-based estimates of $\Delta_t C_{ant}$ compare overall well with the regional data-based analyses along the cruise transects conducted so far, both in terms of the vertical distributions and the column inventories. The estimated inventory change between 1990 and 2010 reported for the Pacific Ocean on the basis of a small subset of cruises(*43*) is equivalent to a mean storage rate of 0.8±0.2 Pg C yr^{-1} over the 1994 to 2007 period, statistically indistinguishable from ours (1.0±0.1 Pg C yr^{-1}). A similar conclusion is reached in the Atlantic, where the extrapolation of four repeated cruise tracks(*61*) yields a storage rate of 0.6±0.1 Pg C yr^{-1}, which is somewhat smaller than ours (0.9±0.1 Pg C yr^{-1}). A recent North Atlantic estimate(*31*) of 0.39 Pg C yr^{-1} (north of 25°N including the Arctic) is nearly identical to our estimate of 0.38±0.03 Pg C yr^{-1} in the same region.

There is less agreement with the only other global attempt to estimate the change in ocean carbon storage based on DIC data so far(*67*). This study, which is based on an extrapolation of the changes in DIC diagnosed at a few locations around the world, suggested substantially larger changes in ocean storage (2.9 to 3.4 Pg C yr^{-1}) than our value of 2.5±0.3 Pg C yr^{-1}. However, given the limited dataset used in the former global estimate, its sampling bias and associated extrapolation uncertainties may explain the difference. In contrast, our data-based storage rates for the period 1994 to 2007 are in good agreement with those recently inferred from a diagnostic model of the ocean circulation, where the circulation pattern was analysed separately for the 1990s and the first decade of the 2000(*21*) (Figure S6).

Estimating the scaling factor:

We employ the transient steady-state model(*27*) to estimate the expected change in the oceanic storage of anthropogenic CO_2 between two time points (t_1 and t_2). This model predicts a linear proportionality between this change, $\Delta_t C_{ant}(t_2\text{-}t_1)$, and the amount of anthropogenic CO_2 already present in the water column at time t_1, $C_{ant}(t_1)$, with a proportionality factor, α, i.e., $\Delta_t C_{ant}(t_2\text{-}t_1) \approx \alpha \cdot C_{ant}(t_1)$.

The transient steady-state model is applicable if two conditions are met: (i) The forcing has to be exponential with a constant growth rate, and (ii) the time period of interest is far along into the perturbation such that the contribution of the initial conditions has become negligible. In the case of the oceanic uptake of anthropogenic CO_2, the second condition is clearly met, while this is only partially the case for the first one. This is due to atmospheric CO_2 having nearly doubled its exponential growth rate around the middle of last century, with the exponential rate λ having increased from about 0.01 yr^{-1} to about 0.02 yr^{-1}. Since it takes about $1/\lambda \approx 50$ y for a system to reach the new transient steady state, this condition is just barely met for the 1994 to 2007 period. Thus, we consider the transient steady-state model as an appropriate approach to estimate the expected change in storage, but recognize that we are somewhat fortunate, since this approach would have been problematic if we had tried to apply it to an earlier period.

We estimate the proportionality factor from the relative change in atmospheric CO_2, taking into consideration the change in the surface ocean buffer (Revelle) factor(*68*) and the presence of a growing air-sea disequilibrium(*45*, *69*), which reflects the fact that the surface ocean is closely but not completely following the atmospheric perturbation. The derivation starts with the change in surface ocean *DIC*, i.e., $\Delta_t C_{ant}$, driven by the increase in atmospheric CO_2. Using the same equation as above for $\Delta_t C_{ant}^{eq}$, but extending it to include the presence of a disequilibrium gives:

$\Delta_t C_{ant}(t_2\text{-}t_1) \approx 1/\gamma(t_1..t_2)\ DIC/pCO_2 \cdot \Delta_t pCO_2^{atm}(t_2\text{-}t_1) \cdot \xi(t_1..t_2)$,

where the disequilibrium ratio ξ is the ratio of the change in the oceanic pCO_2, $\Delta_t pCO_2(t_2\text{-}t_1)$ over that in the atmosphere, $\Delta_t pCO_2^{atm}(t_2\text{-}t_1)$. For the Revelle factor $\gamma(t_1..t_2)$, we use its average over the period t_1 to t_2. The scaling factor α can then be estimated from the ratio of the changes between two time periods:

$\alpha = \Delta_t pCO_2^{atm}(t_2\text{-}t_1)/\Delta_t pCO_2^{atm}(t_0\text{-}t_1) \cdot \xi(t_1..t_2)/\xi(t_0..t_1) \cdot \gamma(t_0..t_1)/\gamma(t_1..t_2)$.

Thus, α depends primarily on the ratio of the change in atmospheric CO_2, but is modified by the changes in the buffer factor and the changes in the disequilibrium.

For the period t_1 = t(1994) to t_2 = t(2007) relative to the preindustrial t_0 = t(1750), the ratio of the changes in atmospheric pCO_2 is 0.32 (t_0 = 280 ppm, t_1 = 358 ppm, t_2 = 383 ppm)(*37*) with a very small uncertainty of about ±0.01. The buffer factor γ varies strongly with the seawater chemistry, namely the ratio of DIC and Alk(*11*), but it turns out that the ratio of its changes varies very little between different water masses. Taking the buffer factor for 1950 for $\gamma(t_0..t_1)$ and that for 2000 for $\gamma(t_1..t_2)$ yields a ratio $\gamma(t_0..t_1)/\gamma(t_1..t_2)$ of 0.94 for the mean ocean and low latitude ocean, and a ratio of 0.92 for the high latitude ocean. These buffer factors were computed by using the CO_2 chemistry software package CO2SYS(*64*) and inputting mean surface ocean properties for ~1994(*11*), and scaled DIC values for the respective years. The uncertainty of the computation of the buffer factors is very low, but given their variability in time and space, we assign an uncertainty of ±0.02 to the ratio $\gamma(t_0..t_1)/\gamma(t_1..t_2)$. Assuming a change in the disequilibrium of about 6 µatm between the preindustrial and 1994 and about 3 µatm between 1994 and 2007 yields a ratio $\xi(t_1..t_2)/\xi(t_0..t_1)$ of 0.94. This ratio is rather sensitive to the exact choices of the not well constrained disequilibria, so that we assign it an uncertainty of ±0.05. Using this value plus the buffer factor ratio for the high latitudes and the atmospheric pCO_2 change ratio gives then for α a value of 0.28±0.02 with the majority of the uncertainty stemming from the disequilibrium ratio. Figures S7 and S8 show that the main pattern of anomalous storage are not affected by the uncertainty of the scaling factor, i.e., α = 0.26 yields very similar results as α = 0.30. Also the very small spatial variability of α matters little, since this leads to only very small errors in the anomalous change in C_{ant}, $\Delta_t C_{ant}^{anom}$ (Figure S9). Finally, Figure S10 also reveals that using an alternative estimate for the anthropogenic CO_2 storage in 1994, i.e., by using the ocean inversion based estimate of ref (*14*) instead of the C*-based estimate by ref(*1*) has a relatively small impact on the estimated large-scale distribution of $\Delta_t C_{ant}^{anom}$. The same conclusion applies when the expected change in anthropogenic CO_2 is directly taken from the ocean inversion model rather than estimated by scaling the 1994 result (compare panels c and d in Figure S10).

Estimating the anomalous outgassing of natural CO_2:

We use the surface ocean pCO_2-based air-sea CO_2 flux estimate of ref (*39*) for the period 1994 through 2007 and added a steady-state outgassing of river derived CO_2 of

0.65 Pg C yr^{-1} (average of refs *42*, *43*) in order to obtain the net ocean uptake flux for this period. This estimate includes the both the uptake of anthropogenic CO_2 from the atmosphere as well as any anomalous outgassing of natural CO_2. We then used two approaches to isolate the latter.

In the first approach, we used this adjusted CO_2 flux in 1994, assumed that it constitutes only the anthropogenic CO_2 uptake flux, and then scaled it forward in time using the transient steady-state scaling used above based on atmospheric CO_2 in order to obtain a timeseries of the expected anthropogenic CO_2 uptake flux. In the second approach, we used the estimated anthropogenic uptake flux from the ocean inversion of ref(*17*) for the year 2000 and also used the transient steady-state scaling to scale it forward and backward to obtain a full timeseries of the anthropogenic uptake flux. The anomalous outgassing of flux of natural CO_2 was then computed by subtracting these two expected anthropogenic CO_2 uptake fluxes from the net uptake flux. These two approaches yielded nearly identical integrated losses of natural of CO_2 of 5±3 Pg C for the period 1994 until 2007. We assign an uncertainty of ±60% to this value given the large number of assumptions that go into this estimate. The most important source of uncertainty in the first approach is the assumption that the anomalous flux of natural CO_2 is zero in 1994, while the largest source of uncertainty for the second approach is the magnitude of the river-derived CO_2 outgassing.

References:

49. R. M. Key *et al.*, A global ocean carbon climatology: Results from Global Data Analysis Project (GLODAP). *Global Biogeochem. Cycles*. **18** (2004), doi:10.1029/2004GB002247.

50. T. Tanhua *et al.*, Atlantic Ocean CARINA data : overview and salinity adjustments. *Earth Syst. Sci. Data*, 17–34 (2010).

51. R. M. Key *et al.*, The CARINA data synthesis project: introduction and overview. *Earth Syst. Sci. Data*. **2**, 105–121 (2010).

52. K. Suzuki, T., Ishii, M., Aoyama, A., Christian, J. R., Enyo, L. A. Kawano, T., Key, R. M., Kosugi, N., Kozyr, A., Miller, S. Murata, A., Nakano, T., Ono, T., Saino, T., Sasaki, K., C. L. D., Takatani, Y., Wakita, M., and Sabine, "PACIFICA Data Synthesis Project" (2013), doi:10.3334/CDIAC/OTG.PACIFICA_NDP092.

53. S. K. Lauvset *et al.*, A new global interior ocean mapped climatology: The 1°x1° GLODAP version 2. *Earth Syst. Sci. Data*. **8**, 325–340 (2016).

54. R. A. Locarnini *et al.*, "World Ocean Atlas 2013, Volume 1: Temperature" (2013).

55. M. M. Weng *et al.*, "World Ocean Atlas 2013: Volume 2: Salinity" (2013).

56. M. AOYAMA *et al.*, Current Status of Homogeneity and Stability of the Reference Materials for Nutrients in Seawater. *Anal. Sci.* **28**, 911–916 (2012).

57. R. E. Sonnerup, P. D. Quay, A. P. McNichol, The Indian Ocean ^{13}C Suess Effect. *Global Biogeochem. Cycles*. **14**, 903–916 (2000).

58. Y. Plancherel, K. B. Rodgers, R. M. Key, a. R. Jacobson, J. L. Sarmiento, An assessment of regression methods used to measure changes in the oceanic distribution of anthropogenic carbon. *Biogeosciences*. **10**, 4801–4831 (2013).

59. N. Gruber, J. L. Sarmiento, in *THE SEA: Biological-Physical Interactions in the Oceans*, A. R. Robinson, J. J. McCarthy, B. J. Rothschild, Eds. (John Wiley and Sons, New York, 2002), vol. 12, pp. 337–399.

60. A. C. Martiny *et al.*, Strong latitudinal patterns in the elemental ratios of marine plankton and organic matter. *Nat. Geosci.* **6**, 279–283 (2013).

61. R. J. Woosley, F. J. Millero, R. Wanninkhof, Rapid anthropogenic changes in CO_2 and pH in the Atlantic Ocean: 2003-2014. *Global Biogeochem. Cycles*. **30**, 70–90 (2016).

62. W. S. Broecker, S. Blanton, W. M. Smethie, G. Ostlund, Radiocarbon decay and oxygen utilization in the deep Atlantic Ocean. *Glob. Biogeochem. Cycles*. **5**, 87–117 (1991).

63. B. I. McNeil, R. J. Matear, R. M. Key, J. L. Bullister, J. L. Sarmiento, Anthropogenic CO_2 Uptake by the Ocean Based on the Global Chlorofluorocarbon Data Set. *Science (80-.).* **299**, 235–239 (2003).

64. S. van Heuven, D. Pierrot, J. W. B. Rae, E. Lewis, D. W. R. Wallace, CO2sys: MATLAB Program Developed for CO_2 System Calculations. (2011), , doi:10.3334/CDIAC/otg.CO2SYS_MATLAB_v1.1.

65. C. Mehrbach, C. H. Culberson, J. E. Hawley, R. M. Pytkowicz, Measurement of the apparent dissociation constants of carbonic acid in seawater at atmospheric pressure. *Limnol. Ocean.* **18**, 897–907 (1973).

66. A. G. Dickson, F. J. Millero, A comparison of the equilibrium constants for the dissociation of carbonic acid in seawater media. *Deep Sea Res.* **34**, 1733–1743 (1987).

67. S. Kouketsu, A. M. Murata, Detecting decadal scale increases in anthropogenic CO_2 in the ocean. *Geophys. Res. Lett.* **41**, 4594–4600 (2014).

68. J. L. Sarmiento, C. LeQuéré, S. W. Pacala, Limiting future atmospheric carbon dioxide. *Glob. Biogeochem. Cycles*. **9**, 121–137 (1995).

69. K. Matsumoto, N. Gruber, How accurate is the estimation of anthropogenic carbon in the ocean? An evaluation of the ΔC* method. *Global Biogeochem. Cycles*. **19** (2005), doi:10.1029/2004GB002397.

70. L. Resplandy *et al.*, Revision of global carbon fluxes based on a reassessment of oceanic and riverine carbon transport. *Nat. Geosci.* **11** (2018), doi:10.1038/s41561-018-0151-3.

71. A. R. Jacobson, S. E. Mikaloff Fletcher, N. Gruber, J. L. Sarmiento, M. Gloor, A joint atmosphere-ocean inversion for surface fluxes of carbon dioxide: 1. Methods and global-scale fluxes. *Global Biogeochem. Cycles*. **21**, 1–13 (2007).

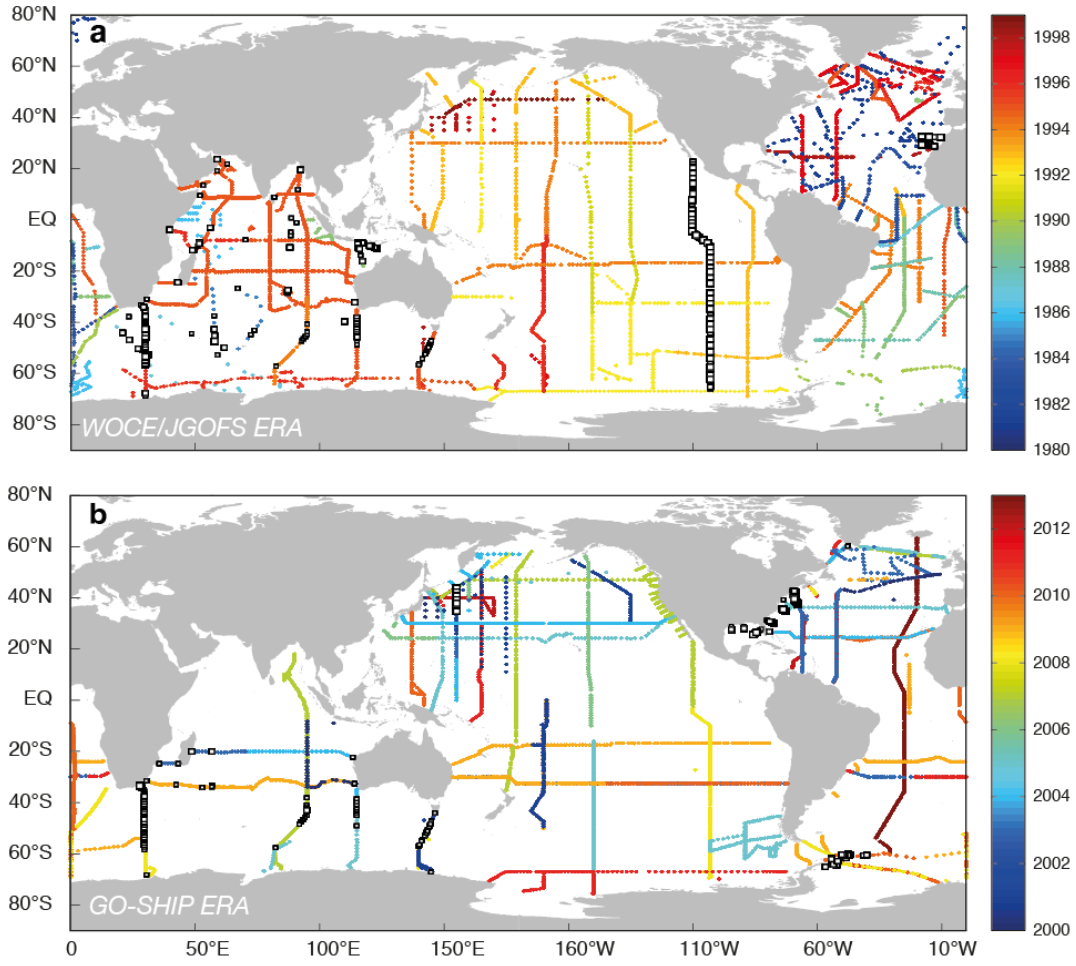

Fig. S1.

Maps of the sampling locations of the data used for the two eras: (a) for the WOCE/JGOFS era (1982 to 1999) and (b) as (a), but for the Repeat Hydrography/GO-SHIP era (from 2000 to 2013). The colors of the filled dots indicate the year of sampling. Open squares indicate stations/cruises that are in GLODAPv2, but not used for our analyses (see text for details). The size of the squares indicates the number of samples affected: Small: 0-9 samples, Medium: 10-19 samples, Large >19 samples. Stations that were sampled more than once during the Repeat Hydrography/GO-SHIP era are shown with two colors and with the second occupation plotted on top.

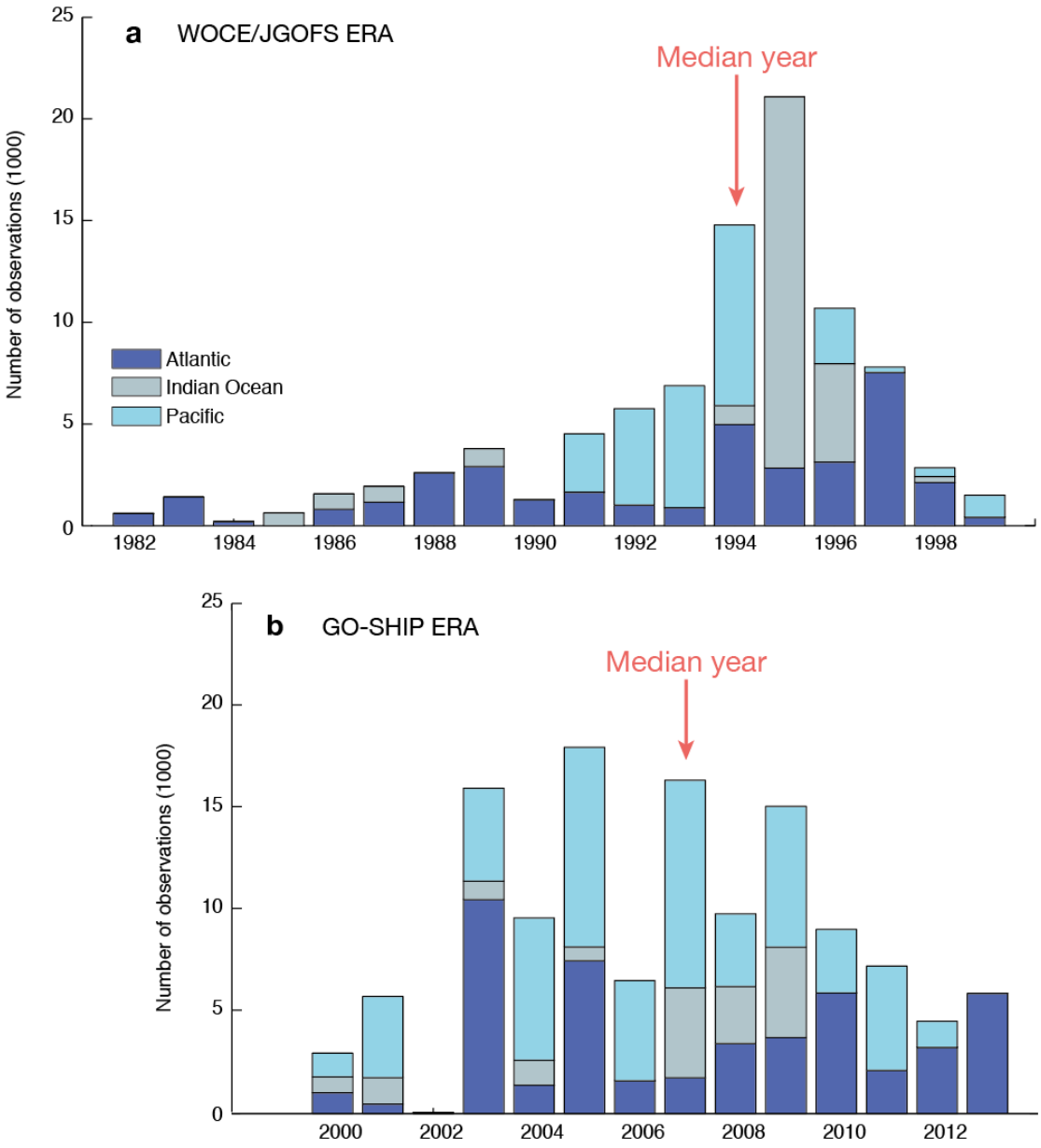

Fig. S2.

Distribution of the data through time. Shown are the number of discrete samples of C* for each year and basin that were used to construct the two multiple linear regression models.

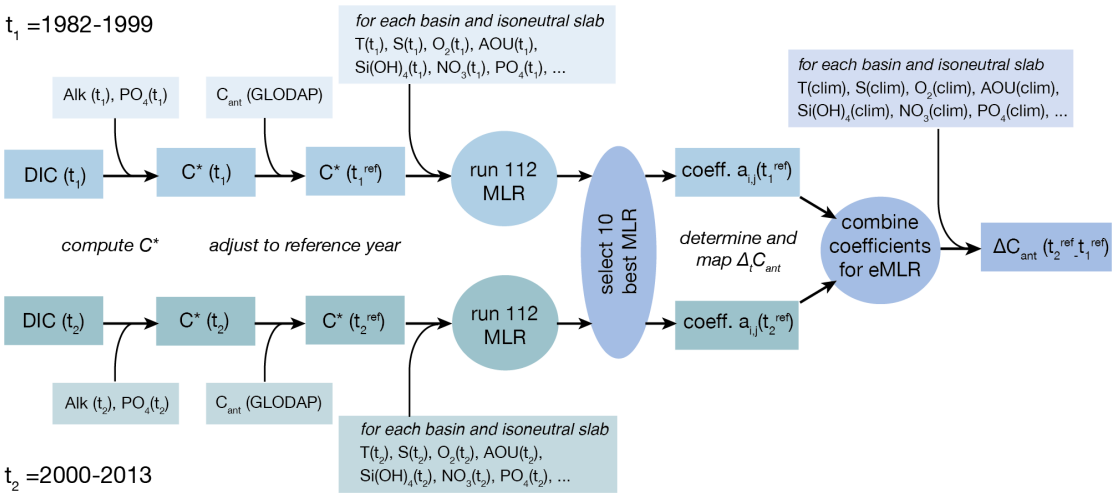

Fig. S3.

Procedure to estimate the change in anthropogenic CO_2 between the JGOFS/WOCE and the GOSHIP eras in the water column below 150 m. Adapted from ref(*9*).

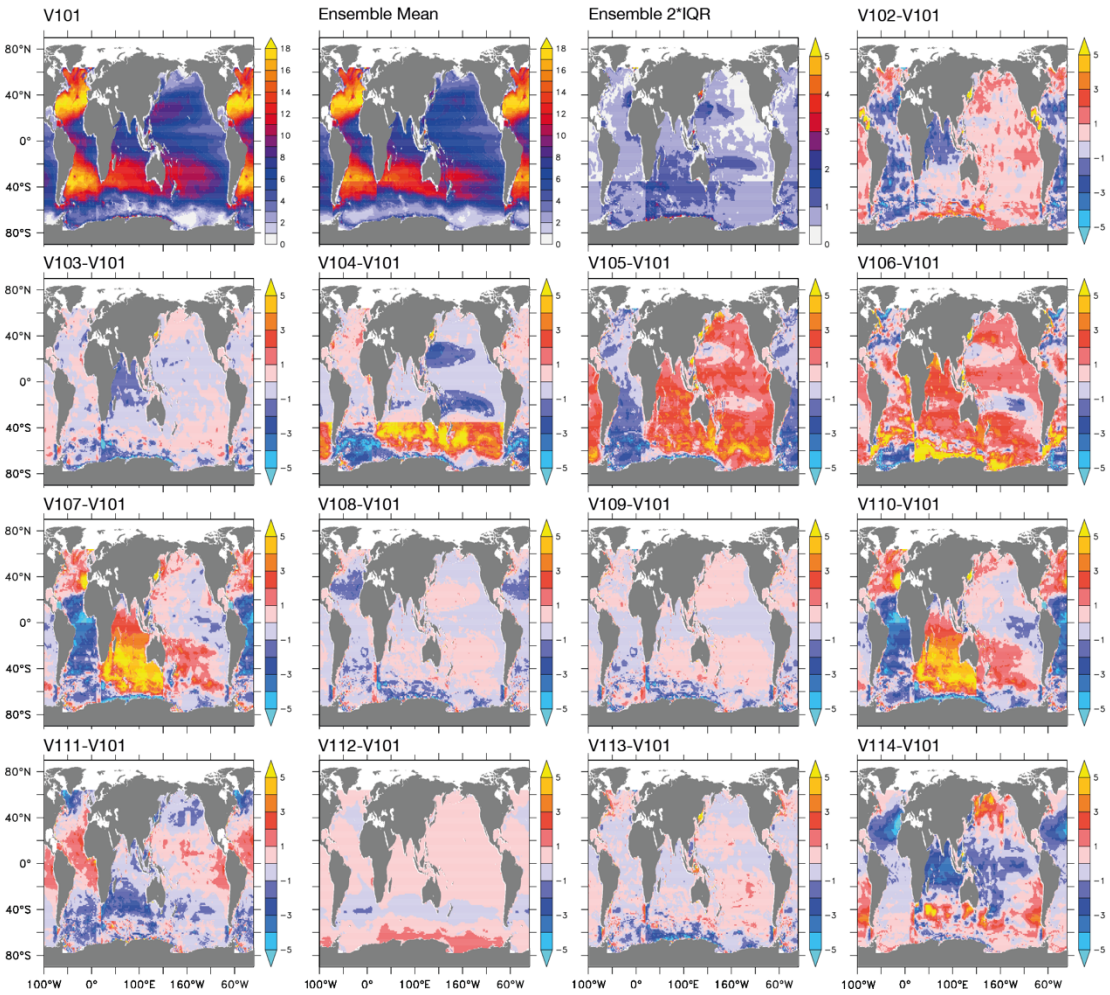

Fig. S4.

Column inventories of the change in anthropogenic CO_2 (mol m^{-2}) (0-3000 m) between 1994 and 2007 of the standard case and of the 13 sensitivity cases considered. Also shown are the ensemble mean of the 14 cases and twice their interquartile range. For V102 through V114, the difference to the standard case V101 is shown. (See Table S1 for a full description of these sensitivity cases).

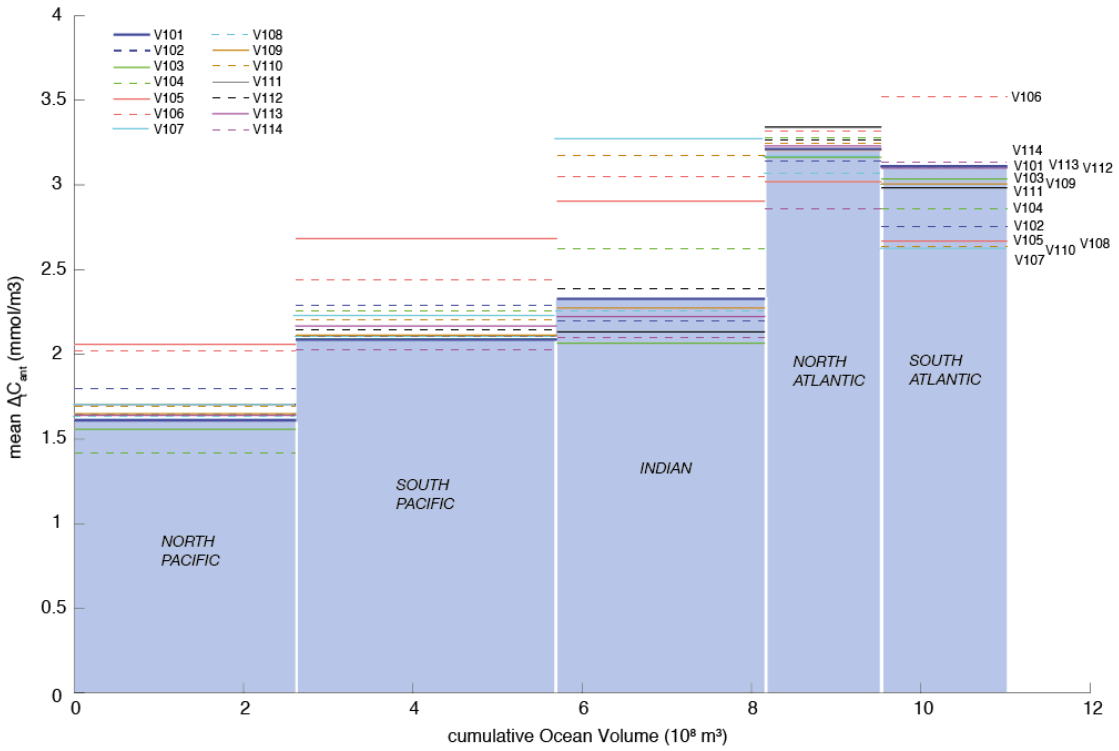

Fig. S5.

Inventories (0-3000 m) for the standard case as well as for the 13 sensitivity cases considered. Shown is the mean change in the concentration of anthropogenic CO_2 in the respective ocean basins as a function of the ocean volume. Thus, the area of the rectangle for each ocean basin is directly proportional to the total inventory change for this ocean basin.

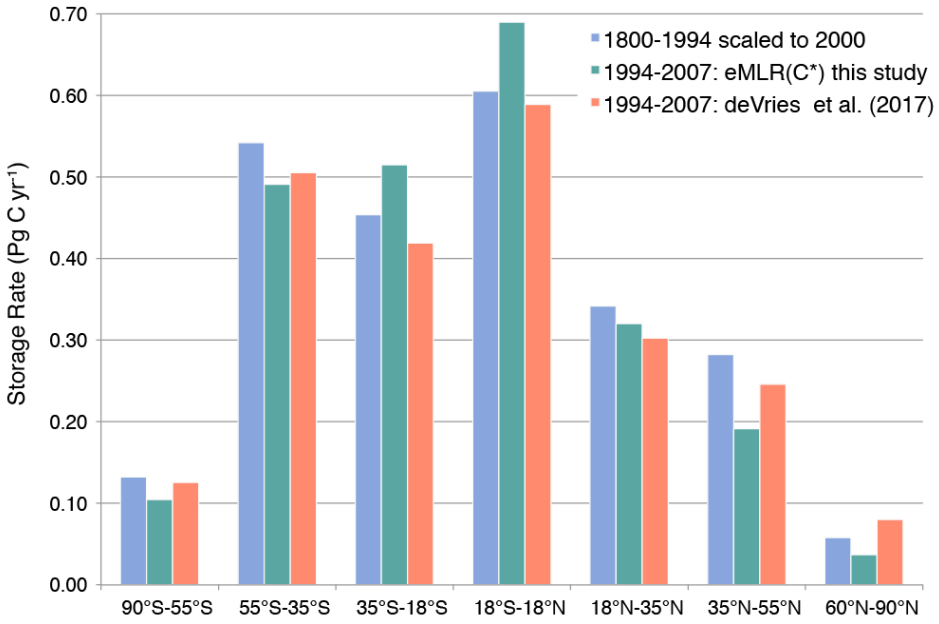

Fig. S6.

Comparison of the mean storage rate of anthropogenic CO_2 between 1994 and 2007 for the global ocean w/o the Arctic Ocean and the Mediterranean Sea. Shown are three estimates: The C* method-based estimate for the period 1800 to 1994(*1*) scaled to 2000 (blue) (see text), the eMLR(C*) based estimate (green), and a diagnostic model-based estimate(*21*), the latter interpolated to the 1994 to 2007 period. The uncertainties of the C*-based estimates are about 20%, those of the eMLR(C*) based estimates about ±10%, and those for the diagnostic model are reported to be less than 5%(*21*).

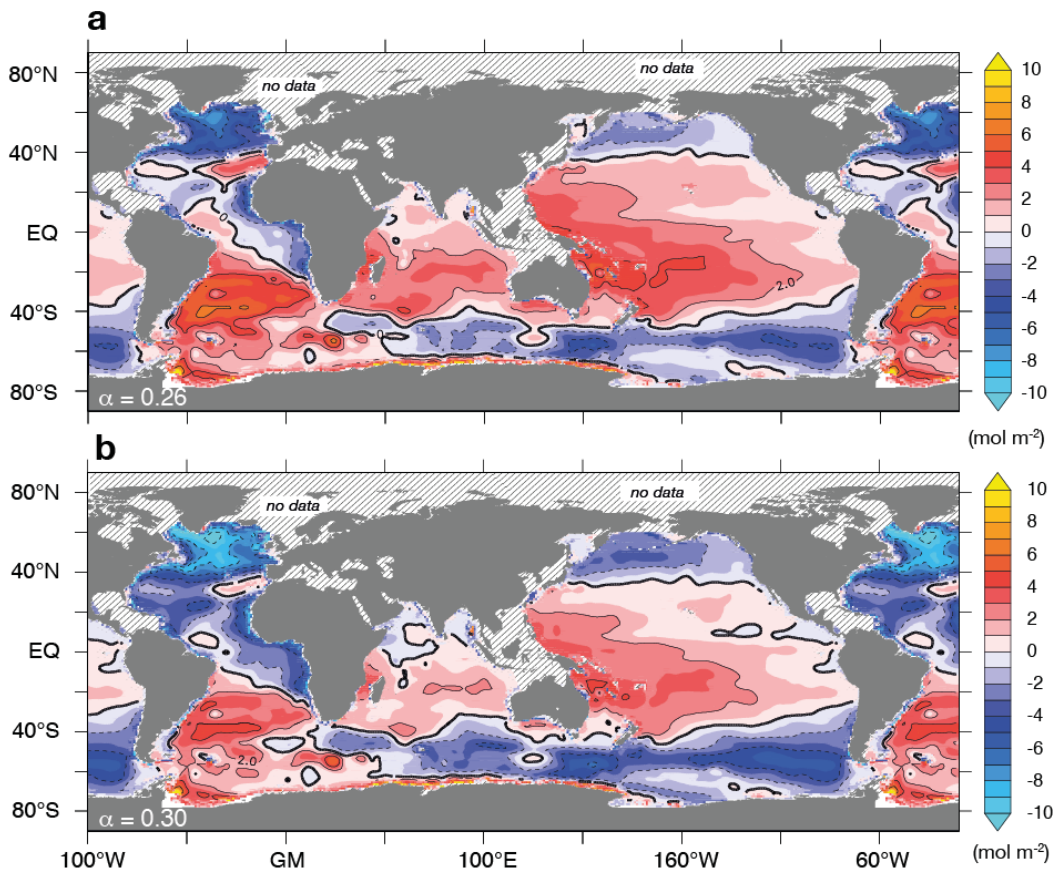

Fig. S7.

Sensitivity of anomalous change in storage to the value of the scaling factor α: (a) α = 0.26 (lower bound estimate), and (b) α = 0.30 (upper bound estimate).

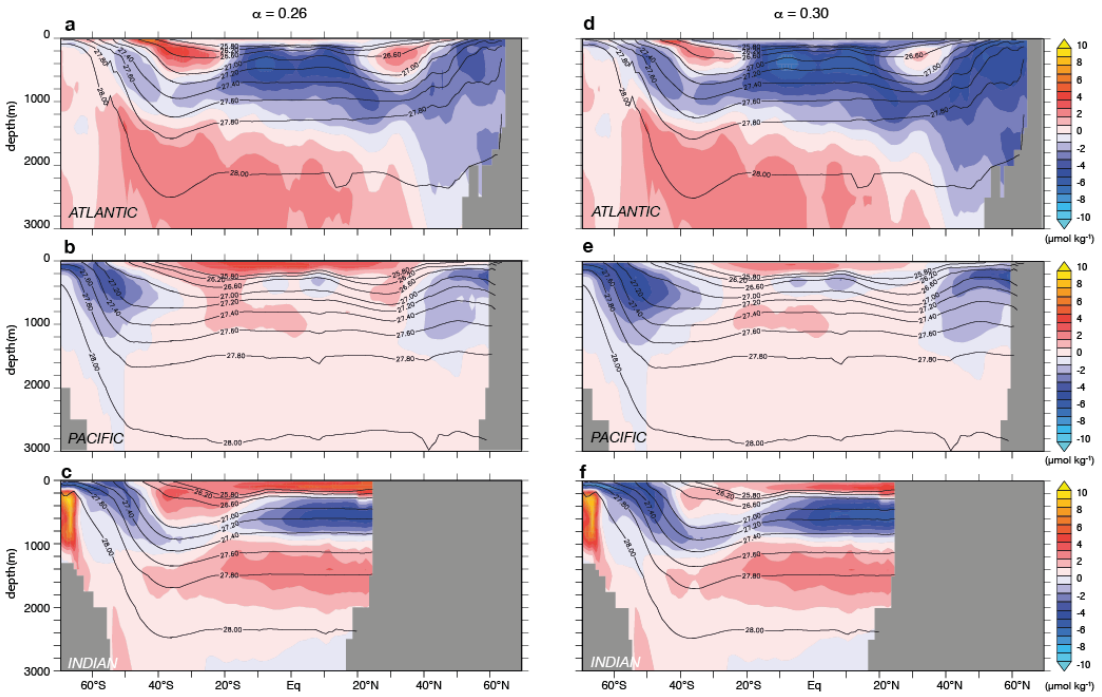

Fig. S8.

Sensitivity of anomalous change in the zonal mean sections of $\Delta_t C_{ant}$ to the value of the scaling factor α: (a-c) $\alpha = 0.26$ (lower bound estimate), and (d-f) $\alpha = 0.30$ (upper bound estimate). (a, b): Atlantic Ocean, (b,e): Pacific Ocean, and (c,f): Indian Ocean..

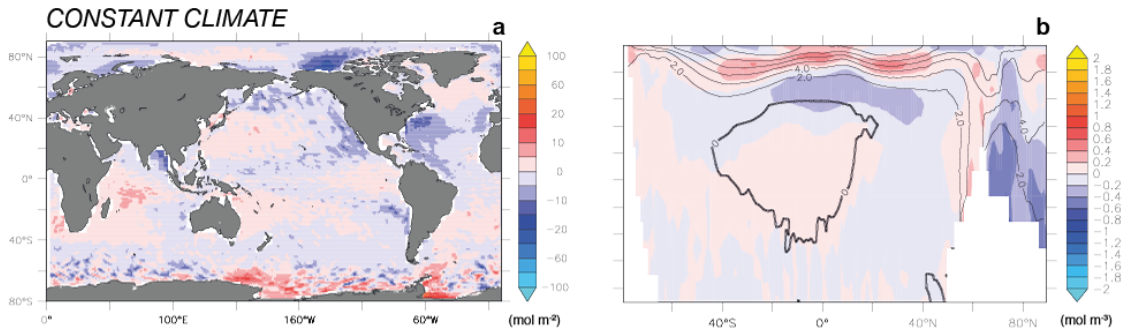

Fig. S9.

Assessment of the impact of the spatial variations in the scaling factor α on the estimated $\Delta_t C_{ant}^{anom}$. (a) Column inventory of the error in $\Delta_t C_{ant}^{anom}$, and (b) zonal mean section of the error in $\Delta_t C_{ant}^{anom}$. The anomalous change in both panels was computed assuming a constant scaling factor α of 0.25, i.e., $\Delta_t C_{ant}^{anom} = \Delta_t C_{ant} - 0.25 \cdot C_{ant}(1994)$ using the constant climate results from the hindcast simulations with the NCAR CCSM described in detail in (*9*).

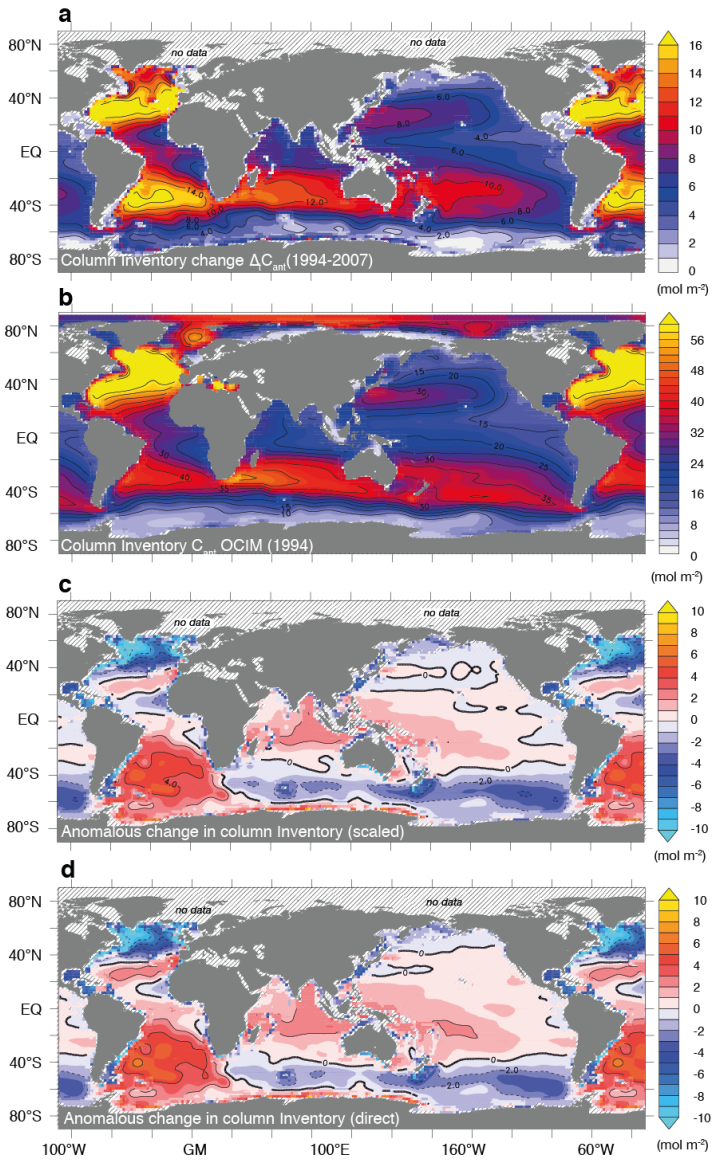

Fig. S10.

As Figure 3 in the main text, except for panel b showing the ocean inversion-based (OCIM) carbon inventory of anthropogenic CO_2 for the year 1994 from ref (*14*) instead of the C*-based estimate from ref (*1*), and panel c showing the anomalous change in Δ_tC_{ant} computed by subtracting the OCIM inventory for 1994 instead of the C*-based one, i.e, $\Delta_tC_{ant}^{anom}$(scaled) = Δ_tC_{ant}(eMLR, 1994-2007) – 0.28*C_{ant}(OCIM, 1994). The additional panel d shows the anomalous change in Δ_tC_{ant} when the expected change in Δ_tC_{ant} between 1994 and 2007 is taken directly from the OCIM simulated change, i.e., $\Delta_tC_{ant}^{anom}$(direct) = Δ_tC_{ant}(eMLR, 1994-2007) – Δ_tC_{ant}(OCIM, 1994-2007). To compute $\Delta_tC_{ant}^{anom}$ for the OCIM-based estimates, the Δ_tC_{ant} estimates were interpolated onto the 2°x2° of the OCIM estimates. The similarity of panels c and d with panel c of Figure 3 in the main text indicates that $\Delta_tC_{ant}^{anom}$ is neither sensitive to the choice of the C_{ant} fields for 1994 nor to the assumption of a constant scaling factor α=0.28.

Table S1.

Neutral density slabs used for the eMLR(C*) method to determine the change in anthropogenic CO_2 and selection of predictors in the multiple linear regressions (MLR)[a]:

Isoneutral range	Temp.	Sal.	*AOU*	PO_4^{3-}	NO_3^-	$Si(OH)_4$	PO_4*
Atlantic density intervals							
<26.00	8	5	7	6	2	5	7
26.00-26.50	7	8	6	6	3	3	7
26.50-26.75	9	7	5	5	3	1	9
26.75-27.00	10	3	5	5	4	6	6
27.00-27.25	8	2	4	5	4	9	7
27.25-27.50	8	3	8	7	4	4	6
27.50-27.75	6	4	8	9	4	3	5
27.75-27.85	4	3	8	9	7	4	5
27.85-27.95	3	10	5	8	4	5	5
27.95-28.05	3	10	6	9	2	2	6
28.05-28.10	10	5	6	4	3	2	9
28.10-28.15	8	7	6	6	1	3	8
28.15-28.20	8	5	7	8	1	4	6
>28.20	5	10	3	8	3	0	4
Indo-Pacific density intervals							
<26.00	8	4	7	4	8	2	6
26.00-26.5	9	4	4	5	2	7	8
26.50-26.75	7	3	6	6	7	2	8
26.75-27.00	6	2	7	7	6	2	9
27.00-27.25	4	10	7	7	2	3	6
27.25-27.50	5	7	7	8	2	3	8
27.50-27.75	8	7	6	6	1	3	8
27.75-27.85	10	5	3	3	3	5	7
27.85-27.95	7	4	6	6	2	7	7
27.95-28.05	4	6	9	9	2	5	4
28.05-28.10	1	4	8	8	3	9	6
>28.10	2	4	7	8	3	9	7

(a) Shown is number of times this variable is part of the 10 best MLR regressions

Table S2.

List of the sensitivity cases considered. V101 is the standard case.

Identi–fier	Description	Number of regions	Number of iso slabs	Variables	Data source	Data mapping	Surface method
101	**Standard Case**	**2**	**14 + 12**	**all**	**GLODAP2+**	**WOA &GLODAP**	**combined**
102	only WOA (No GLODAP)	2	14 + 12	all	GLODAP2+	WOA only	combined
103	no PO4*	2	14 + 12	all wo PO4*	GLODAP2+	WOA &GLODAP2	combined
104	Southern Ocean	3 + S. Oce.	14 + 12	all	GLODAP2+	WOA &GLODAP2	combined
105	upper ocean: two regions; lower ocean: one region	2+1	14 + 12	all	GLODAP2+	WOA &GLODAP2	combined
106	only Carter variables†	2	14 + 12	Carter variables	GLODAP2+	WOA &GLODAP2	combined
107	5 regions	5	14 + 12	all	GLODAP2+	WOA &GLODAP2	combined
108	no A16 2013	2+1	14 + 12	all	GLODAP2 wo A16	WOA &GLODAP2	combined
109	reduced number isopycnal, 2 regions	2	10 + 8	all	GLODAP2+	WOA &GLODAP2	combined
110	reduced number isopycnal, 5 regions	5	10 + 8	all	GLODAP2+	WOA &GLODAP2	combined
111	no sfc equ	2	14 + 12	all	GLODAP2+	WOA &GLODAP2	eMLR only
112	global sfc equ	2	14 + 12	all	GLODAP2+	WOA &GLODAP2	surface equilibrium only
113	C* based on NO3	2	14 + 12	all	GLODAP2+	WOA &GLODAP2	combined
114	all data GLODAP2	2	14 + 12	all	GLODAP2	WOA &GLODAP2	combined

† Only the variables used by Carter et al. (*43*) are used as predictors in the eMLRs.

Table S3.

Reconstructed column inventories (0-3000m) in the different ocean basins for each of the sensitivity cases listed in Table S2. Note that this table includes just the inventories for the regions mapped by the eMLR(C*) method, i.e., the numbers here neither include the Arctic and other marginal seas nor the ocean below 3000m.

Version	North Atlantic (Pg C)	South Atlantic (Pg C)	North Pacific (Pg C)	South Pacific (Pg C)	Indian (Pg C)	Global (Pg C)
101 (Std)	**5.3**	**5.6**	**5.2**	**8.0**	**7.1**	**31.2**
102	5.2	5.0	5.8	8.7	6.7	31.4
103	5.3	5.5	5.0	8.0	6.4	30.1
104	5.5	5.1	4.6	8.6	8.0	31.9
105	5.1	4.8	6.6	10.1	8.7	35.3
106	5.5	6.3	6.5	9.3	9.3	36.9
107	5.3	4.7	5.4	8.5	9.7	33.5
108	5.1	5.4	5.3	8.0	6.9	30.7
109	5.4	5.4	5.3	8.1	7.0	31.2
110	5.4	4.7	5.4	8.4	9.4	33.2
111	5.5	5.4	5.3	7.9	6.4	30.5
112	5.4	5.6	5.3	8.2	7.3	31.7
113	5.4	5.6	5.3	8.2	6.8	31.3
114	4.7	5.5	5.1	7.8	6.5	29.6
Median	**5.3**	**5.4**	**5.3**	**8.2**	**7.0**	**31.3**
IQR	**0.2**	**0.5**	**0.2**	**0.6**	**1.8**	**2.0**